Bidisperse Mixtures Of Colloidal Rods In A Dipolar External Field

Joost de Graaf

28.06.2006

Bachelor Thesis
Supervisor dr. R.H.H.G. van Roij
Institute for Theoretical Physics
Utrecht University

Contents

Abstract

Onsager theory is applied to determine the external field dependence of the isotropic-nematic coexistence relations for binary mixtures of thick and thin hard dipolar colloidal rods with a diameter ratio of 1/3. The approximation in this thesis neglects dipole-dipole interactions. Starting from a non-ideal gas virial expansion, we develop Onsager theory and apply it to colloidal rods. We use numerical integration techniques to solve the associated non-linear differential equation for monodisperse systems in order to find the angular distribution. A Newton-Raphson procedure is employed to determine the coexistence relations. From this limiting monodisperse case, the theory for bidisperse systems is derived. Finally the results obtained for the above mentioned system are analysed.

Preface

This thesis has been written with third year Bachelor students in mind, therefore some of the introductory material may seem redundant to more experienced readers and it can be easily skipped. We have assumed some basic thermodynamic knowledge, see [1] and [2] for instance, and aim not to get bogged down in the mathematical details of the preliminaries to the results. Mathematics is seen as a tool, not as a means to an end.

This text can be divided into three parts. Intending to describe bidisperse systems of colloidal rods and their field dependence, we start by developing Onsager theory in the first. To that end non-ideal gas theory is considered and a semi-grand canonical approach is used to obtain a virial theory for suspensions and solutions. The main focus of the second part will be the analysis of the results for monodisperse systems, as monodisperse systems are a limiting case for bidisperse ones. We start by applying Onsager theory to colloidal rods. Pausing briefly to examine the mathematical properties of such systems and discuss the numerical approximation schemes used to solve the equations, before moving on to the analysis of the results. Here we focus mainly on the limitations of the model and their implications for possible experimental verification. In the third part the monodisperse relations are extended to a set of equations governing the behaviour of bidisperse systems. After a minimum of mathematical analysis, the adaptations needed to make the numerical approximation schemes suitable are treated. We then arrive at the crux of this thesis, the description and analysis of the results for bidisperse systems obtained using these techniques. Finally an outlook is presented on further study in this particular segment of colloidal science.

Chapter 1

Introduction

Thermodynamics is the cumulation of centuries of experimental and theoretical work, resulting in the combination of both the statistical and the mechanical disciplines. From a strong empirical base, founded by the work of Kelvin, Joule and many others, a mathematical framework was developed by men such as Boltzmann and Gibbs. Today Thermodynamics is one of the best established classical theories. It is of such elegance and applicability that A. Einstein remarked: “It is the only physical theory of universal content which I am convinced will never be overthrown, within the framework of applicability of its basic concepts.” A remarkable feature of macroscopic systems, consisting of say 10^{23} atomic coordinates, is that they can be described using only a few macroscopic coordinates, i.e. pressure, temperature etc. Thermodynamics is the study of the 10^{23} hidden coordinates. Using statistical methods this theory allows us to derive the relatively simple relations governing the behaviour of macroscopic systems, with which we are familiar form Mechanics and Chemistry. Such a simplification is a recurring element in Thermodynamics and it can be used to great advantage in describing a multitude of physical properties, in this case those of colloidal rod suspensions.

Colloids are mesoscopic particles in the nm-μm size range, which makes them larger than most molecules, but still small enough to exhibit significant Brownian motion. These particles are ‘soft’ condensed[1] matter, a term which refers to the ease with which such systems are compressed and deformed compared to traditional condensed matter. Non-spherical colloids form liquid crystal phases. Liquid crystals have many applications in modern technology, i.e. LCDs, LC-thermometers. These substances have properties which differ from atomic matter. They can flow as a liquid and scatter light as a crystal, hence their name. In addition, colloids allow for real time tracking of inter particle interactions via microscopy, which is much more difficult if not impossible in molecular systems. Their crystalline phase can be used to create so-called photonic bandgap materials, which are the photon equivalent of semiconductors. These properties and applications have sparked interest in colloidal systems and describing their behaviour is of utmost importance to scientists, developers and manufacturers.

Colloids come in many different shapes and sizes, some of which have an orientation, such as rods and platelets. We know that for orientation independent interactions there are at least three phases a system can exhibit: gas, liquid and crystalline[2]. Directional interactions introduce extra phases however. In this thesis we will focus on colloidal rods, such as the rod-like Tobacco Mosaic Virus. Because of their orientability, rods display a whole range of additional phases such as isotropic, nematic and smectic, see figure 1.1. We are most interested in the nematic phase. The system does not have any broken translational symmetries in this phase, but the rods are pointing on average in one direction, the so-called nematic director. In the smectic phase the system forms a kind of layer cake, having broken translational symmetry in one dimension and it is homogeneous in each layer. There are many kinds of

---

[1] Condensed matter is matter in which the number of constituents is extremely large and the interactions between the constituents are strong, i.e. fluids and solids.

[2] Other phases we could consider are the metastable and amorphous phase, both which occur only in certain substances, such as steel and glass respectively.

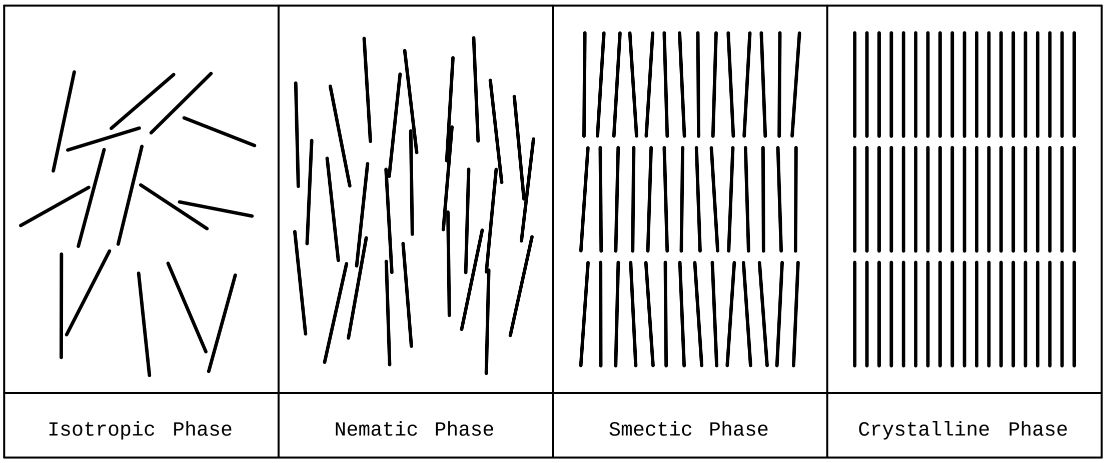

Figure 1.1: Some of the phases a suspension of colloidal rods can exhibit. From left to right in ascending order of concentration. Reproduced from [2] with the author's permission.

smectics, of which smectic-A and smectic-B phase are the most familiar. At first glance the introduction of such a directional dependence seems to complicate theoretical modeling severely. However a relatively simple technique, namely that of Onsager, can be applied to achieve realistic approximations.

Chapter 2

Statistical Mechanics of Interacting Particles

2.1 The Non-Ideal Gas

This section is intended as a refresher into non-ideal gas theory, in particular virial expansions. We aim to be as concise as possible, only touching the mathematics required to rigorously derive the virial expansion. For those who are interested in a more in-depth analysis we recommend [3] and [4]. It should be possible to determine the virial coefficients from the derivation given in this thesis, although this will require significant effort on the part of the reader.

A non-ideal gas is a system of N particles enclosed in a volume V. These particles experience particle-particle interactions, which sets non-ideal gasses apart from ideal ones. The Hamiltonian describing a non-ideal gas consists of a kinetic energy term, an interaction term and possibly an external field term. It can be written as

$$H(\vec{r},\vec{p}) = \sum_{i=1}^{N}\left(\frac{|\vec{p}_i|^2}{2m} + V(\vec{r}_i,\vec{p}_i)\right) + \sum_{1\leq i<j\leq N} \Phi(|\vec{r}_{ij}|), \tag{2.1}$$

where $\vec{r} = (\vec{r}_1,\ldots,\vec{r}_N)$, $\vec{p} = (\vec{p}_1,\ldots,\vec{p}_N)$, $\vec{r}_{ij} = \vec{r}_i - \vec{r}_j$ and Φ is the particle-particle interaction potential. Note that we have tacitly assumed that all particles are the same, the interaction is only distance and not orientation or momentum dependent, and there are only particle-particle interactions. The contribution of complex interactions involving multiple particles is neglected. These assumptions form a substantial simplification, but it will do for our purposes. If there is no external field, we may use equation (2.1) to write the canonical partition function as

$$Z(N,V,\beta) = \frac{1}{N!\Lambda^{3N}} \int_V \mathrm{d}\tau_1 \cdots \int_V \mathrm{d}\tau_N \prod_{1\leq i<j\leq N} \exp(-\beta\Phi(|\vec{r}_{ij}|)),$$

with the inverse temperature $\beta = 1/k_BT$, the thermal wavelength $\Lambda = \sqrt{2\pi\hbar^2\beta/m}$ and with $\mathrm{d}\tau_i$ a volume element, i.e. $\mathrm{d}\tau_i = \mathrm{d}x_i\mathrm{d}y_i\mathrm{d}z_i$ in Cartesian coordinates. Now introduce the so-called Mayer functions $f_{ij} \equiv f(|\vec{r}_{ij}|) = \exp(-\beta\Phi(|\vec{r}_{ij}|)) - 1$ and the configurational integral

$$Q(N,V,\beta) = \int_V \mathrm{d}\tau_1 \cdots \int_V \mathrm{d}\tau_N \prod_{1\leq i<j\leq N} \exp(-\beta\Phi(|\vec{r}_{ij}|)). \tag{2.2}$$

Expand the integrand of $Q(N,V,\beta)$ as

$$\begin{aligned}
\prod_{1\le i<j\le N} \exp(-\beta\Phi(|\vec{r}_{ij}|)) &= \prod_{1\le i<j\le N} (f_{ij}+1) \\
&= 1 + \sum_{\forall(i,j)\in\xi} f_{ij} + \sum_{l=2}^{N(N-1)/2} \sum_{\forall(i_1,j_1)<\cdots<(i_l,j_l)} f_{i_1 j_1}\cdots f_{i_l j_l} \\
&= 1 + \sum_{1\le i<j\le N} f_{ij} + \sum_{\substack{1\le i,j,n,m\le N \\ j<n;\, i=m \\ i<j,\, i<m,\, m<n}} f_{ij}f_{mn} + \cdots , \qquad (2.3)
\end{aligned}$$

where $(i,j) \in \xi \equiv \{(a,b) \in \mathbb{N}\times\mathbb{N} \mid 1 \le a < b \le N\}$ and ξ is a lexicographically ordered set with the order $(i,j) < (m,n) \Leftrightarrow (i < m) \vee ((i = m) \wedge (j < n))$. The term $\forall(i_1,j_1) < \cdots < (i_l,j_l)$ indicates that we have to sum over all possible combinations of indices satisfying this condition. This result is intuitively clear and quite easily derived when one considers this product of $(f_{ij}+1)$-terms, written in a lexicographically ordered tree structure

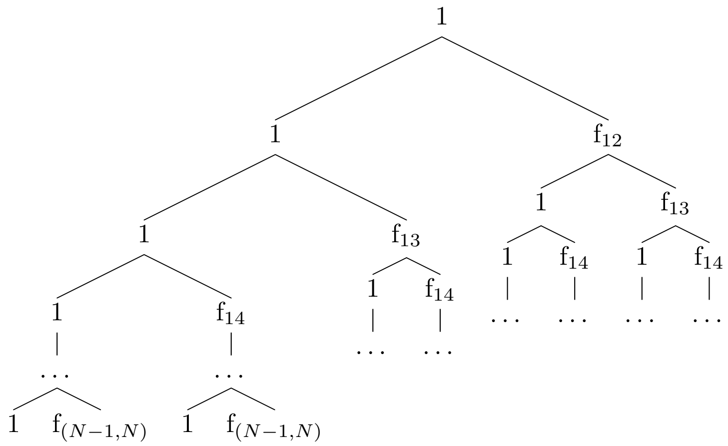

with $f_{ij} \in \{f_{12}, f_{13}, \ldots, f_{(1,N)}, f_{23}, \ldots, f_{(2,N)}, \ldots, f_{(N-1,N)}\}$. Note that all possible f_{ij} are taken into account, each branch terminates in either 1 or $f_{(N-1,N)}$, and the tree is indeed ordered. Furthermore $N(N-1)/2$ is the maximum number of f_{ij} terms, which can be seen by examining the rightmost branch. The above expansion is given by the sum of the path products for all possible downward paths through the tree. The path product is the product of all terms encountered along a path, for instance $1 \cdot f_{12} \cdot 1 \cdot \ldots \cdot f_{89} \cdot \ldots \cdot 1$. This path approach to the expansion explains the sum in line two of equation (2.3). By pulling the integration through this equation[1], we arrive at an expression for $Q(N,V,\beta)$ and hence $Z(N,V,\beta)$ can be written as

$$\begin{aligned}
Z(N,V,\beta) &= \frac{V^N}{N!\Lambda^{3N}} \cdot (1+s) \\
s &\equiv \frac{s_1}{V} + \frac{s_2}{V^2} + \cdots , \qquad (2.4)
\end{aligned}$$

with s_i related to integrals over Mayer functions. When $s \in]-1,1[$ we may use the Taylor expansion of the logarithm and a Stirling approximation to obtain an expression for $F(N,V,\beta)$ in terms of the density $\rho = N/V$. Here we also use the fact that in integration over the whole space many terms are the same, giving us factors N. Then

$$f(\rho,\beta) \equiv \frac{\beta F(N,V,\beta)}{V} = \rho\log(\rho\Lambda^3) - \rho + B_2(\beta)\rho^2 + \frac{B_3(\beta)}{2}\rho^3 + \cdots , \qquad (2.5)$$

for s sufficiently small. Here the B_is are virial coefficients, we will come back to these later. Determining the conditions for which $|s| < 1$ is quite tricky, because one needs to consider equation (2.4) in its

---

[1] This is a legal operation, because the integrand is a finite sum consisting of products of Mayer functions.

entirety, which is a rather horrendous affair. There are a couple of things that help us though. The Mayer functions $f_{ij} \to -1$ for low temperatures and in areas of high potential/interaction strength, usually when the distance between particles is small. Furthermore $f_{ij} \to 0$ for areas of low potential (large distance between particles i and j) and for high temperatures. A general rule of thumb is that $|s| < 1$ if Φ drops off sufficiently fast compared to the volume in which the gas is enclosed and the concentration is not too high. In fact it is easily proven that this is the case for physical interaction potential types in a macroscopic volume, which fall off faster than $1/r^3$, and screened potentials. Now the expression for $F(N, V, \beta)$, equation (2.5), can be used to derive the pressure

$$\beta(P(N, V, \beta) - P_{ID}) = B_2(\beta)\rho^2 + B_3(\beta)\rho^3 + \cdots , \tag{2.6}$$

where $\beta P_{ID} = \rho$ is the ideal-gas pressure. The first few B_i can be found by taking the first terms of s and substituting them in the above equations. Fortunately this has already been done and there even exist formal expressions which generate virial coefficients [5]. The first few are given by:

$$B_2(\beta) = -\frac{1}{2V}\int_V \mathrm{d}\tau_1 \int_V \mathrm{d}\tau_2 \; f(r_{12})$$

$$= -\frac{1}{2V}\int \mathrm{d}\tau_1 \mathrm{d}\tau_2$$

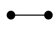

$$B_3(\beta) = -\frac{1}{3V}\int_V \mathrm{d}\tau_1 \int_V \mathrm{d}\tau_2 \int_V \mathrm{d}\tau_3 \; f(r_{12})f(r_{13})f(r_{23})$$

$$= -\frac{1}{3V}\int \mathrm{d}\tau_1 \mathrm{d}\tau_2 \mathrm{d}\tau_3$$

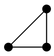

$$B_4(\beta) = -\frac{1}{8V}\int \mathrm{d}\tau_1 \mathrm{d}\tau_2 \mathrm{d}\tau_3 \mathrm{d}\tau_4 \; \Bigl(3$$

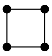

$$+6$$

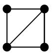

$$+$$

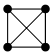

$$\Bigr).$$

The graph notation introduced above is a shorthand developed to write down higher virial coefficients. This notation follows naturally for the lexicographical order imposed on the f_{ij} earlier. It can also be proven that all the diagrams appearing in the virial coefficients are doubly connected. This means that they do not fall apart into disjoined graphs when a single vertex is deleted. Some textbooks do not mention the lexicographical order on the Mayer functions and work completely from a graph-theoretical outset, the two approaches are however equivalent. The above method utilises a canonical approach to the virial expansion, a grand canonical path can also be followed, which leads to the same results. In the grand canonical case the configurational integral $Q(N, V, \beta)$, equation (2.2), are used extensively; this is why they have been introduced here. In both cases the expansion is obtained via the Mayer functions and the Taylor series of the logarithm.

The mathematical derivation of the virial expansion as presented above, was first given by Mayer and Mayer in the 1940's. The f_{ij}s were named in their honour. Virial expansions, in the form of equation (2.6), were originally conceived by Kamerlingh Onnes around 1901, when he considered an improvement to the ideal gas law. He sought to provide better correspondence between theory and experiment at high densities, in much the same way as Van der Waals did in 1873. Since the 1940's the mathematical derivation of virial expansions has become more streamlined and the use of this method is nowadays widely spread. There are some drawbacks to this technique though. Foremost among these is the temperature dependence of the B_is. It entails that for all but the most simple of interactions one needs to recalculate the B_is whenever the the temperature changes. In addition, depending on the system being considered, we may require more than 7 coefficients to achieve a reasonable approximation. Especially in the case of extremely dense gasses, or liquids, with an atomic packing fraction over 0.5. This is less then desirable as the number of cluster integrals[2] increases exponentially for higher coefficients. Clearly virial expansions are a useful tool and can be a powerful technique, but a technique with severe limitations.

---

[2] Integrals over graphs, obtained from the Mayer function integrals.

2.2 Non-Ideal Solutions and Suspensions

For a solution or suspension there is an additional complexity one does not experience with gasses or liquids. One has to deal with at least two types of particles, those of the solvent and those of the solute. The methods used here closely follow those of Ref. [6]. For non-ideal gas mixtures of s different species, we may write the partition function as

$$Z(\vec{N},V,\beta)=\int_V\left(\prod_{i=1}^{s}\frac{\mathrm{d}\tau_i^{N_i}}{N_i!\Lambda_i^{3N_i}}\right)\exp(-\beta\Phi(\vec{r}_1^{N_1},\ldots,\vec{r}_s^{N_s})),$$

with $\vec{N}=(N_1,\ldots,N_s)$, $\vec{r}_i^{N_i}=(\vec{r}_1,\ldots,\vec{r}_{N_i})$ and $\Phi(\vec{r}_1^{N_1},\ldots,\vec{r}_s^{N_s})$ the interaction part of the Hamiltonian, which consists of sums over particle-particle interaction terms. For low densities $\rho_i=N_i/V$ the virial expansion is easily seen to be

$$f(\vec{\rho},\beta)\equiv\frac{\beta F(\vec{N},V,\beta)}{V}=\sum_{i=1}^{s}\rho_i(\log(\rho_i\Lambda_i^3)-1)+\sum_{i,j=1}^{s}B_2^{ij}(\beta)\rho_i\rho_j+\frac{1}{2}\sum_{i,j,k=1}^{s}B_3^{ijk}(\beta)\rho_i\rho_j\rho_k+\cdots, \tag{2.7}$$

where the B_i are the analogue of the monodisperse virial coefficients. There is however a problem when one tries to apply this result directly to solutions or suspensions, namely that the density of the solvent is generally much higher than that of the solutes. This would require the use of far more virial coefficients than desirable to describe the behaviour of the solutes accurately. The solvent would always contribute the dominant part of the virial coefficients, even though it is not particularly relevant to us. It is possible to derive a virial expression, which works around this problem, using a semi-grand canonical approach. We treat the solutes canonically and the solvent grand canonically, hence the name semi-grand canonical. Suppose that species s is the solvent. One may then write the partition sum as

$$\begin{aligned}\exp(-\beta\Omega) &= \sum_{N_s=0}^{\infty}\exp(\beta\mu_s N_s)Z(\vec{N},V,\beta)\\ &= \int\left(\prod_{i=1}^{s-1}\frac{\mathrm{d}\tau_i^{N_i}}{N_i!\Lambda_i^{3N_i}}\right)\sum_{N_s=0}^{\infty}\frac{\exp(\beta\mu_s N_s)}{N_s!\Lambda_s^{3N_s}}\int\mathrm{d}\tau_s^{N_s}\exp(-\beta\Phi(\vec{r}_1^{N_1},\ldots,\vec{r}_s^{N_s}))\\ &\equiv \int\left(\prod_{i=1}^{s-1}\frac{\mathrm{d}\tau_i^{N_i}}{N_i!\Lambda_i^{3N_i}}\right)\exp(-\beta\Phi^{\text{eff}}(\vec{r}_1^{N_1},\ldots,\vec{r}_{s-1}^{N_{s-1}});\mu_s;\beta),\end{aligned} \tag{2.8}$$

where we have introduced Φ^{eff} as the effective interaction between the solute species at given μ_s and β, the chemical potential of the solvent and the inverse temperature respectively. Φ^{eff} is a combination of the interactions the solutes would experience in vacuum and the interaction of the solutes with the solvent. Van Roij proposes the following method to simplify the calculation of the Φ^{eff}. When one considers only the solvent with no solutes, we know that the $\Omega=\Omega_0\equiv-p_0(\mu_s,\beta)V$, where p_0 is the pressure of that system. Now successively consider the cases where there is only one particle present $\Omega=\Omega_0+\omega_i(\mu_s,\beta)$, where there are two particles present, etc. Here ω_i is the potential excess due to the addition of a single particle of species i. For two particles of species i and j the grand potential $\Omega=\Omega_0+\omega_i+\omega_j+\omega_{ij}(r_{ij};\mu_s;\beta)$, where ω_{ij} is the effective pair interaction between species i and j. Continuing in this way we find

$$\begin{aligned}\Phi^{\text{eff}} &= \Omega_0+\Omega_1+\Omega_2+\cdots\\ &= -p_0(\mu_s,\beta)V+\sum_{i=1}^{s}N_i\omega_i(\mu_s,\beta)+\sum_{i,j=1}^{s}\left(\sum_{k_i=1}^{N_i}\sum_{\substack{k_j\neq k_i\\ k_j=1}}^{N_j}\omega_{ij}(r_{k_ik_j};\mu_s;\beta)\right)+\cdots.\end{aligned} \tag{2.9}$$

Ω_0 and Ω_1 are independent of the position of the solute particles. By pulling these position independent factors of equation (2.9) through the integral in equation (2.8), we obtain

$$\begin{aligned} \Omega(N_1,\dots,N_{s_1},\mu_s,V,\beta) &= -p_0(\mu_s,\beta)V+\Omega_1(N_1,\dots,N_{s-1},\mu_s,V,\beta) \\ &\quad +A(N_1,\dots,N_{s-1},\mu_s,V,\beta) \qquad (2.10) \\ \exp(-\beta A) &= \int_V \left(\prod_{i=1}^{s-1}\frac{\mathrm{d}\tau_i^{N_i}}{N_i!\Lambda_i^{3N_i}}\right)\exp(-\beta\Omega_2(\vec{r})+\cdots), \qquad (2.11) \end{aligned}$$

where A is the Helmholtz free energy of the effective canonical $(s-1)$-component system with interaction Hamiltonian $\Omega_2+\cdots$, as defined by equations (2.10) and (2.11). We may now determine the pressure of the system and the chemical potentials for the solute particles via

$$\begin{aligned} p &= -\left(\frac{\partial\Omega}{\partial V}\right)_{\mu_s,\,\beta,\,\vec{N}} \\ &= p_0(\mu_s,\beta)-\left(\frac{\partial A}{\partial V}\right)_{\mu_s,\,\beta,\,\vec{N}} \\ &= p_0(\mu_s,\beta)+\Pi(\rho_1,\dots,\rho_{s-1};\mu_s;\beta) \\ \mu_i &= -\left(\frac{\partial\Omega}{\partial N_i}\right)_{\mu_s,\,\beta,\,\vec{N}-\{N_i\}} \\ &= \omega_i(\mu_s,\beta)+\left(\frac{\partial A}{\partial N_i}\right)_{\mu_s,\,\beta,\,\vec{N}-\{N_i\}} \\ &= \omega_i(\mu_s,\beta)+\mu_i'(\rho_1,\dots,\rho_{s-1};\mu_s;\beta), \end{aligned}$$

where Π is the osmotic pressure, the excess pressure caused by the presence of the solutes, and μ_i' is the i-th solute's excess chemical potential.

What was the point of this calculation? The formulae are not particularly beautiful and determining ω_i and ω_{ij} can be quite tricky. Actually this formalism has a tremendous advantage. When ω_i and ω_{ij} are known, one can treat the solution/suspention as if it the solutes are a gas in vacuum, where the interactions are described by the effective pair potentials. This follows from equation (2.11), in which the canonical partition sum $\exp(-\beta A)$ for the solutes is given. All we have done here is to rewrite the semi-grand canonical function to show that the solutes behave canonically via effective pair interactions. Which enables us to use the multi-component virial expansion on this $\exp(-\beta A)$ term. The presence of the solvent only reveals itself in the μ_s dependence of the free energy, to which the term $\beta\mu_s$ must be added[3]. This term is ignored in the rest of this thesis though, because it is a constant and it does not appear in physical quantities such as the pressure and potential differences. The semi-grand canonical approach allows us to write down a multi-component non-ideal gas virial expansion, substituting pair interactions by effective pair interactions. For most situations one can safely ignore Ω_3 and higher terms. The ability to treat a solution as an effective interaction gas works around the density problem. For low densities this theory yields Van 't Hoff's law: $\beta\Pi=\rho_1+\cdots+\rho_{s-1}$. Now that we have determined the behaviour of virial expansions for suspensions we proceed to use these to derive Onsager theory for colloidal rods in the next chapter.

---

[3] $f_{\mathrm{susp}}=f_{\mathrm{gas}}(\omega_i,\omega_{ij})+\beta\mu_s$.

Chapter 3

Onsager Theory for Monodisperse Rod Systems

3.1 General Derivation without an External Field Interaction

All the theoretical machinery in the previous chapter has been developed under the assumption that the interaction term in the Hamiltonian is independent of the orientation of the particles in space. This is obviously not true in general and it poses a problem if we intend to describe colloidal rods. In the 1940's Lars Onsager introduced a revolutionary approximation technique, which employs orientation independent results to arrive at an expression for orientation dependent systems. He applied this expression to analyse the behaviour of a monodisperse system of hard colloidal rods. In this section we follow Onsager's derivation [7].

Instead of trying to find a completely new approach to the problem of orientation, Onsager used existing virial expansions. He considered every orientation as a separate species, each with its own concentration. For simplicity we will only consider a monodisperse system here, but this result can be easily extended to the more general multi-component case. In three dimensions the orientation of a particle can be described by two angles ϕ and θ in spherical coordinates or an orientation unit vector $\hat{\omega} = (\cos(\phi)\sin(\theta), \sin(\phi)\sin(\theta), \cos(\theta))$ in Cartesian coordinates. Onsager began by partitioning the unit sphere into small areas $\mathrm{d}\omega_i$ centred around s unit vectors $\hat{\omega}_i$, $i \in \{1, \ldots, s\}$. In doing so he obtained s 'different' species of particle each with orientation $\hat{\omega}_i$ and concentration ρ_i. He then applied the multi-component virial expansion, equation (2.7), to this system and obtained

$$f(\vec{\rho}, \beta) = \sum_{i=1}^{s} \rho_i(\log(\rho_i \mathcal{V}) - 1) + \sum_{i,j=1}^{s} B_2^{ij}(\beta)\rho_i\rho_j + \frac{1}{2}\sum_{i,j,k=1}^{s} B_3^{ijk}(\beta)\rho_i\rho_j\rho_k + \cdots, \tag{3.1}$$

where $\mathcal{V}$ is the equivalent of Λ^3. Note that $\mathcal{V}$ is the same for all i, because the system is monodisperse even though we see it as consisting of multiple species. Next, Onsager decided to consider only the terms up to the second virial coefficient in equation (3.1). This may seem to be a rather rough approximation, but it actually works quite well for low concentrations. We will come back to this in the next section. Finally he took the limit $s \to \infty$ and derived the following for the free energy

$$f(\rho(\hat{\omega}), \beta) = \int \mathrm{d}\hat{\omega}\rho(\hat{\omega})(\log(\rho(\hat{\omega})\mathcal{V}) - 1) + \int \mathrm{d}\hat{\omega} \int \mathrm{d}\hat{\omega}' \rho(\hat{\omega}) B_2(\hat{\omega}, \hat{\omega}', \beta)\rho(\hat{\omega}'), \tag{3.2}$$

with the second virial coefficient given by

$$B_2(\hat{\omega}, \hat{\omega}', \beta) = -\frac{1}{2}\int \mathrm{d}\vec{r}\,(\exp(-\beta\phi(\vec{r}, \hat{\omega}, \hat{\omega}')) - 1), \tag{3.3}$$

where ϕ is the interaction potential[1]. Equation (3.2) stands at the foundation of Onsager's theory and from it many real systems can be approximated to a high degree of accuracy. We now proceed to use free energy minimisation to find the most probable distribution $\rho(\hat{\omega})$. To that end functional differentiation is employed and the Lagrange multiplier λ is introduced. For the total density ρ, the condition

$$\int \mathrm{d}\hat{\omega}\rho(\hat{\omega}) = \rho, \tag{3.4}$$

gives us a Lagrange constraint, such that

$$\begin{aligned} \frac{\delta}{\delta\rho(\hat{\omega})}\left(f - \lambda\int \mathrm{d}\hat{\omega}\rho(\hat{\omega})\right) &= 0 \quad \Rightarrow \\ \log(\rho(\hat{\omega})\mathcal{V}) + 2\int \mathrm{d}\hat{\omega}' B_2(\hat{\omega},\hat{\omega}',\beta)\rho(\hat{\omega}') - \lambda &= 0\,. \end{aligned} \tag{3.5}$$

To those unfamiliar with functional differentiation, also known as Fréchet differentiation, we recommend [8]. Alternatively these expressions can be derived using equation (3.1), taking the limit $s \to \infty$ afterwards. The normalisation of equation (3.4) is used to obtain the following expression for the equilibrium distribution

$$\rho(\hat{\omega}) = \frac{\rho\exp\big(-2\int \mathrm{d}\hat{\omega}' B_2(\hat{\omega},\hat{\omega}',\beta)\rho(\hat{\omega}')\big)}{\int \mathrm{d}\hat{\omega}''\exp\big(-2\int \mathrm{d}\hat{\omega}' B_2(\hat{\omega}'',\hat{\omega}',\beta)\rho(\hat{\omega}')\big)}\,.$$

This is a self-consistent non-linear integral equation, because $\rho(\hat{\omega})$ is expressed in terms of itself via an integral form. Note that $\rho(\hat{\omega})$ depends on all orientations, as it should. It is perhaps not immediately obvious, but $\rho(\hat{\omega}) = \rho/4\pi$ is an $\hat{\omega}$ independent solution for any ρ and β. This solution is the distribution in the isotropic phase of the system. This phase is characterised by a completely random distribution of the particles, each direction is equally probable. The isotropic phase has the following free energy

$$f_{\mathrm{iso}}(\rho,\beta) = \rho\left(\log\left(\frac{\rho\mathcal{V}}{4\pi}\right) - 1\right) + \frac{\rho^2}{(4\pi)^2}\int \mathrm{d}\hat{\omega}\int \mathrm{d}\hat{\omega}' B_2(\hat{\omega},\hat{\omega}',\beta).$$

It turns out that for low ρ or high temperatures, the isotropic state is the only state the system can occupy. At higher ρ and/or lower temperatures, we have other solutions. The nature of these depends on the precise form of the $B_2(\hat{\omega},\hat{\omega}',\beta)$, however the distribution $\rho(\hat{\omega})$ of these phases can usually not be found analytically and requires a numerical approximation technique.

3.2 Colloidal Rods

At this point we have yet to make assumptions about the nature of the orientation dependence of the $B_2(\hat{\omega},\hat{\omega}',\beta)$. We choose the specific example of hard colloidal rods. Consider a monodisperse system of colloidal rods suspended in a solvent with volume V. The rods have length L and diameter D. Sometimes spherocylinders (capped rods) are used, but this distinction will not prove relevant in our approximation. Furthermore assume that the pair potential is that of hard body interactions, where

$$\beta\phi_{\mathrm{HB}}(\vec{r},\hat{\omega},\hat{\omega}') = \begin{cases} \infty & \text{if overlap} \\ 0 & \text{otherwise.} \end{cases}$$

Insertion into equation (3.3) shows that $B_2(\hat{\omega},\hat{\omega}',\beta)$ becomes independent of β. For hard body interactions B_2 is related to the so-called excluded volume. The Mayer function $f_{ij} = -1$ if the particles overlap and it is 0 otherwise. This leads an excluded volume, because the B_2 gives the volume one particle excludes for the others. The orientation-dependent excluded volume then becomes

$$B_2(\hat{\omega},\hat{\omega}',\beta) = B_2(\hat{\omega},\hat{\omega}') = \pi LD^2 + L^2D|\sin(\gamma(\hat{\omega},\hat{\omega}'))| + \mathcal{O}(D^3) \approx L^2D|\sin(\gamma(\hat{\omega},\hat{\omega}'))|,$$

---

[1] Or the effective interaction potential, depending on the system being considered.

where $\gamma(\hat{\omega}, \hat{\omega}')$ is the angle between $\hat{\omega}$ and $\hat{\omega}'$ and the approximation $L \gg D$ has been used. At this point we come back to the remark in section 3.1 concerning the higher virial coefficients in Onsager theory. Onsager showed that in the limit $D/L \to 0$ his second virial coefficient approximation is exact. However experiments have shown that a ratio $L/D = 15/1$ is already sufficient to obtain accurate results. From here on assume that we are in this long-rod regime. In addition any boundary problems at $\gamma = 0$ and $\gamma = \pi$ one might expect from our $L \gg D$ approximation can be disregarded, since these are points of measure 0.

Write $\hat{n}$ for the nematic director; recall that this is the direction in which the rods are oriented on average. Since the free energy is not influenced by global rotations, we may align the z-axis with the nematic director, thus taking $\hat{\omega}$ relative to $\hat{n}$. Since $\rho(\hat{\omega})$ has rotational symmetry around $\hat{n}$ as well as reflection symmetry in the xy-plane, one can introduce $\rho(\hat{\omega}) = \rho\psi(\theta)$. Here θ is the polar angle measured from the $\hat{n}$-axis. Equation (3.4) requires

$$\int \mathrm{d}\hat{\omega}\psi(\theta) = \int_0^{2\pi} \mathrm{d}\phi \int_0^{\pi} \mathrm{d}\theta \sin(\theta)\psi(\theta) = 1\,.$$

It is possible to rewrite $|\sin(\gamma(\hat{\omega}, \hat{\omega}'))|$ for our new choice of coordinates as

$$\begin{aligned} |\sin(\gamma(\hat{\omega}, \hat{\omega}'))| &= \sqrt{1 - \cos^2(\gamma(\hat{\omega}, \hat{\omega}'))} \\ &= \sqrt{1 - \langle \hat{\omega}, \hat{\omega}' \rangle^2} \\ &= \sqrt{1 - (\cos(\theta)\cos(\theta') + \sin(\theta)\sin(\theta')\cos(\phi' - \phi))^2}\,. \end{aligned}$$

Introducing the integral kernel

$$\begin{aligned} K(\theta, \theta') &= \int_0^{2\pi} \mathrm{d}\phi' |\sin(\gamma(\hat{\omega}, \hat{\omega}'))| \\ &= \int_0^{2\pi} \mathrm{d}\phi' \sqrt{1 - (\cos(\theta)\cos(\theta') + \sin(\theta)\sin(\theta')\cos(\phi' - \phi))^2}\,, \end{aligned} \tag{3.6}$$

we can write for the free energy

$$\begin{aligned} f(\rho) &= \rho \int \mathrm{d}\hat{\omega}\psi(\theta)(\log(\rho\psi(\theta)\mathcal{V}) - 1) + \frac{\rho^2}{2} \int \mathrm{d}\hat{\omega} \int \mathrm{d}\hat{\omega}'\psi(\theta)B_2(\hat{\omega}, \hat{\omega}')\psi(\theta') \quad \Rightarrow \\ \frac{f(\rho)}{\rho} &= \log(\rho\mathcal{V}) - 1 + \int \mathrm{d}\hat{\omega}\psi(\theta)\log(\psi(\theta)) + \frac{\rho}{2} \int \mathrm{d}\hat{\omega} \int \mathrm{d}\hat{\omega}'\psi(\theta)B_2(\hat{\omega}, \hat{\omega}')\psi(\theta') \\ &= \log(\rho\mathcal{V}) - 1 + 2\pi \int \mathrm{d}\theta \sin(\theta)\psi(\theta)\log(\psi(\theta)) \\ &\quad + 2\pi\frac{\rho}{2}2L^2D \int \mathrm{d}\theta \sin(\theta) \int \mathrm{d}\theta' \sin(\theta')\psi(\theta)K(\theta, \theta')\psi(\theta'), \end{aligned}$$

where the θ integrals are from 0 to π. Henceforth we will omit the boundaries for all the θ integrals. Now choose $\mathcal{V} = \pi L^2 D/4$ and $c = \mathcal{V}\rho$. This choice of $\mathcal{V}$ may seem a bit arbitrary, but it will enable us to write down the formulae in a very clean way. In addition we know that $\mathcal{V}$ does not occur in the expression for $\rho(\hat{\omega})$, nor does it in physical quantities such as the pressure and chemical potential differences. Therefore it is safe to make this choice. When we write $f(c) \equiv f(\rho)/\rho$, substitution of the above mentioned formulae gives

$$\begin{aligned} f(c) &= \log(c) - 1 + 2\pi \int \mathrm{d}\theta \sin(\theta)\psi(\theta)\log(\psi(\theta)) \\ &\quad + 8c \int \mathrm{d}\theta \sin(\theta) \int \mathrm{d}\theta' \sin(\theta')\psi(\theta)K(\theta, \theta')\psi(\theta') \\ \psi(\theta) &= \frac{1}{Z}\exp\left(-\frac{8c}{\pi} \int \mathrm{d}\theta' \sin(\theta')K(\theta, \theta')\psi(\theta')\right) \\ Z &= 2\pi \int \mathrm{d}\theta'' \sin(\theta'')\exp\left(-\frac{8c}{\pi} \int \mathrm{d}\theta' \sin(\theta')K(\theta'', \theta')\psi(\theta')\right). \end{aligned} \tag{3.7}$$

Thus rewriting the free energy $F(N,V,\beta)$ to $f(c)$, a dimensionless free energy dependent on the dimensionless concentration parameter c. Moreover we have found a non-linear integral equation for $\psi(\theta)$. The next section will describe how to solve this type of problem, but first let us derive some additional properties, namely the dimensionless pressure and dimensionless chemical potential.

$$\begin{aligned}
f(c) &= \frac{\beta F}{N}\\
P &= -\left(\frac{\partial F}{\partial V}\right)_{N,\beta}\\
&= -\left(\frac{\partial F}{\partial c}\right)\left(\frac{\partial c}{\partial V}\right)\\
&= \left(\frac{N\mathcal{V}}{V^2}\right)\left(\frac{\partial F}{\partial c}\right)\\
&= \left(\frac{N\mathcal{V}}{V^2}\frac{N}{\beta}\right)\left(\frac{\partial f}{\partial c}\right)\\
&= \left(\frac{c^2}{\beta\mathcal{V}}\right)\left(\frac{\partial f}{\partial c}\right) \quad \Rightarrow\\
p(c) &\equiv \mathcal{V}\beta P\\
&= c^2\left(\frac{\partial f}{\partial c}\right)\\
\mu(c) &\equiv \beta\mu\\
&= f(c) + \frac{p(c)}{c}\,,
\end{aligned}$$

where the derivation of $\mu(c)$ is analogous. Note the following: we have used the derivative to c of $f(c)$ to obtain expressions for $p(c)$ and $\mu(c)$. However, $f(c)$ depends on $\psi(\theta)$ which in turn also depends on c, one could express this as $f(c,\psi(c))$, thus

$$\left(\frac{\mathrm{d}f}{\mathrm{d}c}\right) = \left(\frac{\partial f}{\partial c}\right) + \int \mathrm{d}\hat{\omega}\left(\frac{\delta f}{\delta\psi(\hat{\omega})}\right)\left(\frac{\mathrm{d}\psi(\hat{\omega})}{\mathrm{d}c}\right).$$

Fortunately we need to calculate $p(c)$ and $\mu(c)$ for the ψ which minimises $f(c)$. Therefore $\delta f/\delta\psi = \lambda$, with λ the lagrange multiplier, which implies

$$\int \mathrm{d}\hat{\omega}\left(\frac{\delta f}{\delta\psi(\hat{\omega})}\right)\left(\frac{\mathrm{d}\psi(\hat{\omega})}{\mathrm{d}c}\right) = \int \mathrm{d}\hat{\omega}\lambda\left(\frac{\mathrm{d}\psi(\hat{\omega})}{\mathrm{d}c}\right) = \frac{\mathrm{d}}{\mathrm{d}c}\left(\lambda\int \mathrm{d}\hat{\omega}\psi(\hat{\omega})\right) = \frac{\mathrm{d}}{\mathrm{d}c}(\lambda\cdot 1) = 0\,,$$

and one can write $\partial f/\partial c$ immediately. Remarkably, for hard-rod systems the distribution and all dimensionless physical quantities depend only on one variable, namely the dimensionless concentration c. The temperature only comes into play when the transition from the dimensionless to the normal characterisations of the pressure and chemical potential is made. Evaluating the expression for $p(c)$ yields

$$p(c) = c + 8c^2\int \mathrm{d}\theta\sin(\theta)\int \mathrm{d}\theta'\sin(\theta')\psi(\theta)K(\theta,\theta')\psi(\theta').$$

Finally we introduce the nematic order parameter,

$$S \equiv \langle(3\cos^2(\theta)-1)/2\rangle = 2\pi\int \mathrm{d}\theta\sin(\theta)\psi(\theta)\frac{3\cos^2(\theta)-1}{2}\,.$$

This parameter represents the extent to which the rods are oriented along the nematic director. In the isotropic phase there is no ordering and $S=0$, in the nematic phase S can be as high as 0.99 for almost totally ordered systems. For the isotropic regime the equations derived in this section simplify to

$$
\begin{aligned}
\psi_{\text{iso}}(\theta) &= \frac{1}{4\pi} \\
f_{\text{iso}}(c) &= \log\left(\frac{c}{4\pi}\right) - 1 + c && (3.8) \\
p_{\text{iso}}(c) &= c^2 + c && (3.9) \\
\mu_{\text{iso}}(c) &= \log\left(\frac{c}{4\pi}\right) + 2c && (3.10) \\
S_{\text{iso}} &= 0\,.
\end{aligned}
$$

In the next section we proceed to analyse the nematic phase mathematically and develop techniques to tackle the non-linear integral equation for $\psi(\theta)$.

3.3 Mathematical and Numerical Analysis

We begin this section by examining some of the properties of the non-linear integral equation for the $\psi(\theta)$ distribution

$$\log(4\pi\psi(\theta)) = \lambda - \frac{8c}{\pi}\int \mathrm{d}\theta \sin(\theta)|\sin(\gamma(\hat{\omega},\hat{\omega}'))|\psi(\theta'), \qquad (3.11)$$

where λ is a Lagrange multiplier. The origin of this formula should be obvious as it is merely a reformulation of equation (3.5) for hard colloidal rods. There are basically two methods for approximating a solution to this equation. The first is algebraic in nature, the second is purely numerical.

The distribution $\psi(\theta)$ is invariant under rotations of the reference frame and invariant under azimuthal rotations. Legendre polynomials in $\cos(\theta)$ form a set of eigenfunctions of these operations, the even Legendre polynomials obey the symmetry of the $\psi(\theta)$ distribution, namely $\psi(\theta) = \psi(\pi - \theta)$. The idea behind the mathematical analysis of equation (3.11) is to expand the functions in terms of even Legendre polynomials. This approach was followed by Kayser and Raveché in 1978 [9]. They gave the following expressions:

$$
\begin{aligned}
K(\theta,\theta') &= 2\pi\sum_{n=0}^{\infty} c_{2n}P_{2n}(\cos(\theta))P_{2n}(\cos(\theta')); \\
f(\theta) &= \sum_{n=0}^{\infty} a_{2n}P_{2n}(\cos(\theta)); \\
\log(f(\theta)) &= \sum_{n=0}^{\infty} \alpha_{2n}P_{2n}(\cos(\theta)),
\end{aligned}
$$

where the unknown expansion coefficients a_{2n} and α_{2n} are related via a rather complicated relations, and were the c_{2n} are known. Solving the system obtained by substituting these equations into equation (3.11) however, is far beyond the scope of this text. There are no closed forms for the coefficients a_{2n} as a function of the c_{2n}. Usually an iterative method is employed to approximate these coefficients. Kayser and Raveché used this technique to perform a bifurcation analysis on equation (3.11). There exists at least one solution, namely the isotropic distribution. A bifurcation analysis determines if and where[2] a nematic type solution can branch from the isotropic phase. It is clear that near the branch point we may introduce $\psi(\theta) = (1 + \epsilon h(\theta))/4\pi$, where ϵ is an infinitesimally small value, and $h(\theta)$ is some function orthogonal to $1/4\pi$, by the condition that $\langle\psi\rangle = 1$. Substituting this equation into (3.11), linearising in

---

[2] For what value of the dimensionless concentration c.

ϵ and using a Legendre polynomial expansion yields

$$\begin{aligned} h(\theta) &= -\frac{4c}{\pi}\sum_{n=0}^{\infty} c_{2n} P_{2n}(\cos(\theta))\langle P_{2n}\rangle \\ \langle P_{2n}\rangle &= \int_0^{\pi} \mathrm{d}\theta \sin(\theta) P_{2n}(\cos(\theta)) h(\theta). \end{aligned} \tag{3.12}$$

Kayser and Raveché used even Legendre polynomials as a trial solution for $h(\theta)$, note that equation (3.12) is a self-consistent problem. However these polynomials satisfy this equation only for a specific value of c, say c^*. The lowest of these values taken over all even Legendre polynomials proves to be the location of the bifurcation point. Kayser and Raveché obtained the minimum value $c^* = 4$. We will come back to the physical importance of this concentration when we discuss the monodisperse results in section 3.4.

The second method is purely numerical [10]. This method uses an iterative procedure to obtain $\psi(\theta)$ from an initial guess. The self-consistency requirement is used to improve the initial guess step by step, until equation (3.7) is satisfied. This equation is self-consistent as it expresses $\psi(\theta)$ in terms of itself. Consider a discrete equidistant grid in θ. Let N_θ be the number of θ-values in this grid then for k = 0, 1, . . . , N_θ we have

$$\theta_k = \pi\frac{k}{N_\theta}\ .$$

The $\psi(\theta) = \psi(\pi - \theta)$ symmetry implies that one could suffice with only half the interval in θ, namely $\theta \in [0, \pi/2]$. Requiring only half the number of grid points to obtain the same result would obviously be faster in a computer calculation. However, we plan on introducing a field which breaks this symmetry, thus the full interval length of $[0, \pi]$ is used. A trapezoidal integration scheme allows us to approximate integrals. Let $q(\theta)$ be some function, then

$$\int_0^{\pi} \mathrm{d}\theta \sin(\theta) q(\theta) \approx \sum_{k=0}^{N_\theta} \Delta_k q(\theta_k),$$

where upon using $\mathrm{d}\theta \sin(\theta) = -\mathrm{d}\cos(\theta)$ we find

$$\Delta_k = \begin{cases} 1 - \dfrac{(\cos(\theta_0) + \cos(\theta_1))}{2} & k = 0 \\[2ex] \dfrac{(\cos(\theta_{k-1}) - \cos(\theta_{k+1}))}{2} & k = 1, \ldots, N_\theta - 1 \\[2ex] 1 + \dfrac{(\cos(\theta_{N_\theta - 1}) + \cos(\theta_{N_\theta}))}{2} & k = N_\theta\ . \end{cases}$$

This form for Δ_k guarantees that the $\sum_k \Delta_k = 2$. A similar expression is employed to perform the ϕ integration in the integral kernel, equation (3.6), $K(\theta, \theta') \to K_{kl}$. Note that the kernel does not change during the procedure outlined in the following sections. This means that the two dimensional array need only be calculated once and stored, or it could be fetched from memory if it has been precalculated. This yields

$$\begin{aligned} K_{kl} &= \frac{2\pi}{N_\phi}\left(\frac{1}{2}g_{kl}(\phi_0) + \sum_{j=1}^{N_\phi - 1} g_{kl}(\phi_j) + \frac{1}{2}g_{kl}(\phi_{N_\phi})\right)\ ; \\ g_{kl}(\phi) &= \sqrt{1 - (\cos(\theta_k)\cos(\theta_l) + \sin(\theta_k)\sin(\theta_l)\cos(\phi))^2}\ ; \\ \phi_k &= \frac{2\pi}{N_\phi}k \quad \text{for } k = 0, \ldots, N_\phi\ . \end{aligned}$$

Now introduce an initial guess, a starting point for the iteration. There are two types of initial guess used in this thesis.

1. Isotropic, $\tau_k = 1/4\pi$ for $k = 1, \ldots, N_\theta$. This provides excellent convergence for nearly isotropic distributions, within 1 to 2 iterations. It has slow convergence for strongly nematic phases though. Depending on the concentration as many as 50 iterations might be required.
2. Gaussian[3], $\tau_k = (c/\pi)^2 \exp(-2c^2\theta_k^2/\pi)$ for $k = 1, \ldots, N_\theta/2$ and $\tau_{N_\theta - k} = \tau_k$, which works well for nematic phases. Usually around 10 iterations are required. The Gaussian initial guess can be found by accommodating the function $\gamma \exp(\alpha\theta^2)$ to the free energy, by minimising the discrepancy with the real $\psi(\theta)$ with respect to α and γ. Onsager used the form $\alpha \cosh(\alpha\cos(\theta))/(4\pi\sinh(\alpha))$, with α suitably chosen [11].

We now have all the ingredients to solve the problem iteratively. Start by calculating the following

$$\begin{aligned} A_k &= \frac{8c}{\pi}\sum_{l=0}^{N_\theta} \Delta_l K_{kl} \tau_l && (3.13)\\ Z &= 2\pi \sum_{k=0}^{N_\theta} \Delta_k \exp(-A_k) && (3.14)\\ \psi_k &= \frac{\exp(-A_k)}{Z}\,, && (3.15)\end{aligned}$$

where ψ_k is our new estimate for the distribution function. This procedure constitutes a single iteration. Take $\psi_k \rightarrow \tau_k$ and re-evaluate the expressions (3.13), (3.14) and (3.15). One can continue this way indefinitely. To exit this loop we need a condition, in this case check for self-consistency. Self-consistency is obtained when $\max|\psi_k - \tau_k| < \delta$, with δ a small value. If this condition is satisfied, the ψ_k can be used to calculate $f(c)$, $p(c)$, etc, for which discretised forms of f, p, μ and S are required. Experience teaches us that $N_\theta = N_\phi \approx 40 \sim 80$ gives reasonable results which show good qualitative behaviour, and $N_\theta = N_\phi \approx 200 \sim 400$ gives accurate quantitative results, around $3 \sim 4$ digit precision.

In addition to this iterative scheme we use another numerical technique, namely Newton-Raphson (NR). NR is employed to find points where there is isotropic-nematic coexistence. For coexistence determination one needs to solve the two dimensional system, depending on two variables, c_{iso} and c_{nem}

$$\begin{aligned} p(c_{\text{iso}}) - p(c_{\text{nem}}) &= 0\\ \mu(c_{\text{iso}}) - \mu(c_{\text{nem}}) &= 0\,.\end{aligned}$$

We apply a two dimensional NR-routine to find the c_{iso} and c_{nem}, for which there is coexistence. The implementation of this algorithm is fairly straightforward [12]. It is quite important to have good initial guesses for c_{iso} and c_{nem} though, because the 2D NR-routine has poor convergence. Now that we have discussed the numerical techniques used to derive results, we can describe the results and their implications in the next section. There the additional complexity of an external dipolar field interacting with a moment is also introduced to the problem.

3.4 Numerical Results without an External Field Interaction

The results derived here were obtained using $N_\theta = N_\phi = 500$ and $\delta = 10^{-5}$. In figure 3.1 the $\psi(\theta)$ dependence on c is given, the distribution becomes increasingly peaked for higher values of c. Values between $c = 0.001$ and $c = 4$ have been omitted, because the phases in this range are mostly isotropic and would coincide with the red line. Although not clearly visible, the red line has $\psi(\theta) = 1/4\pi$ within numerical uncertainty everywhere. For high c values $\psi(\theta)$ behaves like two δ-function peaks, one in $\theta = 0$ and the other in $\theta = \pi$, as can be expected. To get a better idea of what happens we examine figure 3.2. The isotropic phase persists to $c = 4.002 \approx 4.0$ and that the nematic phase appears at $c = 3.486 \approx 3.5$. Recall that Kayser and Raveché had determined the branching value $c^* = 4$ analytically, which agrees

---

[3] We may assume N_θ to be even.

with our terminal value for the isotropic phase within the uncertainty. We can now describe the physical significance of this bifurcation point c^*. The nematic phase branches from the isotropic in this point, which means there is another curve joining the point $c = 4.002$ to $c = 3.486$. For the nematic begin point this occurs in a smooth way and at the bifurcation point in a continuous, non differentiable way. Calculation of this curve is quite involved, requiring the methods of Kayser and Raveché, and therefore not performed here. However, an indication of the shape of this curve is given in figure 3.2 (right) using blue points. We can see that the begin point of the nematic phase is not a starting point at all, but a bending point. For values of c exceeding 4.0 the dimensionless concentration is too high to allow a stable isotropic phase to exist.

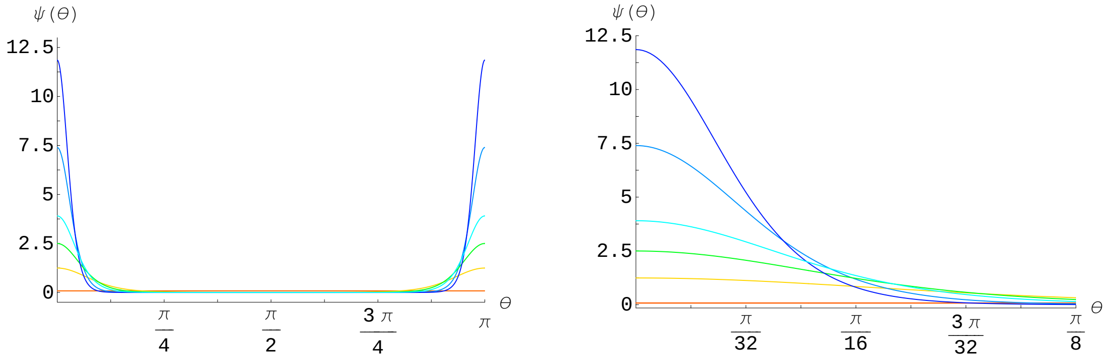

Figure 3.1: The orientation distribution $\psi(\theta)$ for several values of the dimensionless concentration c, from red to blue: $c = 0.001$, 4, 5, 6, 8, 10 (left). Detail (right).

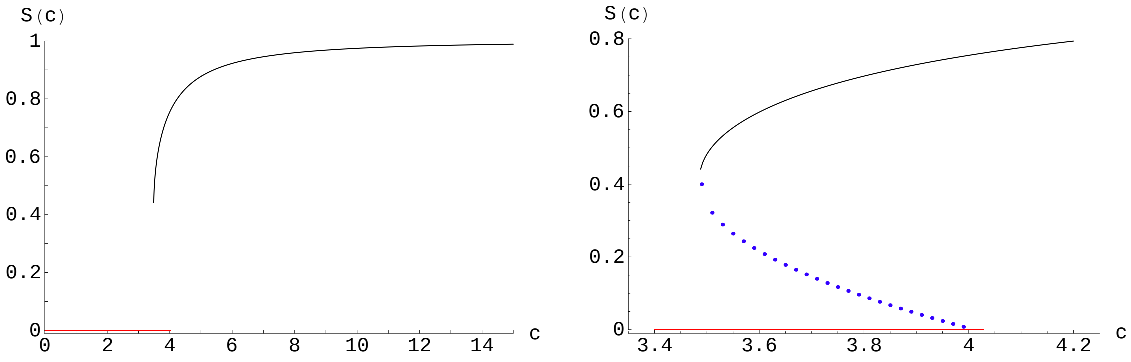

Figure 3.2: The nematic order parameter S as a function of the dimensionless concentration c, the isotropic branch is red and the nematic black (left). Close-up of the graph restricted to the domain $[3.4, 4.2]$ (right). The blue dots give an indication of the shape of the curve connecting the isotropic-nematic branching point ($c = 4$) with the nematic bending point ($c \approx 3.5$). These points only give an indication of this curve, they do **not** give the exact curve as calculated by Kayser and Raveché, Ref. [9]. The isotropic curve extends slightly beyond the branching point, because this plot was generated using a data set with 2 decimal precision.

For the dimensionless free energy, scaled free energy, pressure and chemical potential the results are given by figures 5.1, 5.2, 5.3 and 5.4 respectively, see Appendix A. In all graphs should be a curve connecting the isotropic and nematic branches. The logarithmic properties of $f(c)$ and $\mu(c)$ and the quadratic behaviour of $p(c)$ for the isotropic branch, predicted by equations (3.8) through (3.10), are quite pronounced. In fact the isotropic results agree with these expressions within the numerical uncertainty, five digit precision, for $c \in]0, 15]$. The nematic phase $p(c)$ behaves linearly in c for high concentrations. It can be shown analytically that in the limit $c \to \infty$ this becomes $p(c) = 3c$. Alternatively one can use the Gaussian initial guess, which corresponds closely to the $\psi(\theta)$ distribution at very high c, $c \gg 100$, and determine the pressure dependence numerically, this yields $p(c) = 3.0c$ as well.

Finally we consider the coexistence of an isotropic and a nematic phase. A Maxwell common tangent construction is employed to find coexistence conditions [2]. For coexistence the pressures and the chemical potentials of the phases are equal. We know that $\mu = (\partial F/\partial N)_{V,\beta} = (\partial f/\partial \rho)_\beta$ and $p(\rho) = \rho\mu(\rho) - f(\rho)$. Thus a tangent to the $f(\rho)$ graph will obey

$$\left.\frac{\partial f}{\partial \rho}\right|_{\rho_1} = \left.\frac{\partial f}{\partial \rho}\right|_{\rho_2} = \frac{f(\rho_2) - f(\rho_1)}{\rho_2 - \rho_1} \,,$$

which can be rewritten using the above relations as

$$(\rho_2 - \rho_1)\mu_0 = (f(\rho_2) - f(\rho_1)) + (p_0 - p_0), \tag{3.16}$$

where μ_0 is the coexistence chemical potential and p_0 the coexistence pressure. An adaptation of equation (3.16) yields the following formula $cf(c) - c\mu_0^* + p_0^*$, with μ_0^* the dimensionless coexistence chemical potential and p_0^* the dimensionless coexistence pressure. One now expects this function to have two minima, one for the isotropic and one for the nematic coexistence concentration, both of which lie on the c-axis. The c-axis acts as the tangent in this modified form of the original free energy graph.

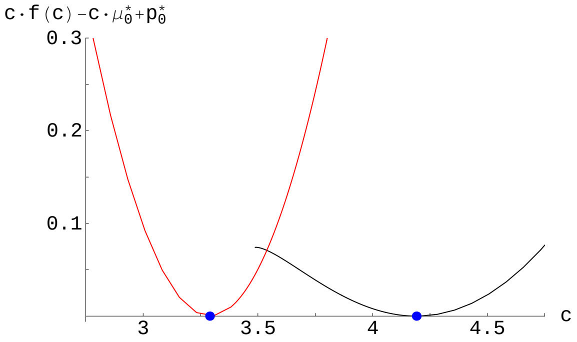

Figure 3.3: A modified dimensionless free energy graph, to which a Maxwell common tangent construction has been applied. The tangent being the c-axis, the dimensionless concentration axis, μ_0^* is the dimensionless chemical potential at coexistence and p_0^* the dimensionless pressure at coexistence. Note that the isotropic coexistence value is given by $c_{\text{iso}}^* \approx 3.3$ and the nematic coexistence value by $c_{\text{nem}}^* \approx 4.2$, indicated by the blue dots.

Figure 3.3 indicates that coexistence occurs at $c_{\text{iso}}^* \approx 3.3$ and $c_{\text{nem}}^* \approx 4.2$. Admittedly, using the coexistence values in the plot is not really possible without prior knowledge, but it does dramatically improve the readability of the graph. Figure 5.2 (left) gives a standard Maxwell common tangent and figure 5.2 (right) an indication of the small isotropic-nematic tangent differences near the coexistence points. Using the NR-technique the following values given in the 5 digit precision are obtained, see the table below.

parameter	value
c_{iso}^*	3.2903
c_{nem}^*	4.1911
f_{iso}^*	.95032
f_{nem}^*	1.8724
$p_{\text{iso}}^* = p_{\text{nem}}^*$	14.117
$\mu_{\text{iso}}^* = \mu_{\text{nem}}^*$	5.2407
S_{iso}^*	.00000
S_{nem}^*	.79222

3.5 Numerical Results with an External Field Interaction

We now consider a monodisperse system of hard dipolar colloidal rods, with the dipole moment along the long axis of the rods. The rods can interact with an external field, but do not exhibit dipole-dipole interactions. The following dipolar interaction potential $\Phi_{\text{ext}}(\theta) = -W\cos(\theta)$ is used. Here $W = mE$, with m the dipole moment and E the field strength. The field is homogeneous and points in the same direction as the nematic director. A simple calculation now gives us the extended forms for ψ, f, μ and p by incorporating this field

$$\begin{aligned}
\psi(\theta) &= \frac{1}{Z}\exp\left(-\frac{8c}{\pi}\int \mathrm{d}\theta' \sin(\theta')K(\theta,\theta')\psi(\theta') + \beta W\cos(\theta)\right) \\
f(c) &= \log(c) - 1 + 2\pi\int \mathrm{d}\theta \sin(\theta)\psi(\theta)\log(\psi(\theta)) \\
&\quad +8c\int \mathrm{d}\theta \sin(\theta)\int \mathrm{d}\theta' \sin(\theta')\psi(\theta)K(\theta,\theta')\psi(\theta') \\
&\quad -2\pi\beta W\int \mathrm{d}\theta \sin(\theta)\cos(\theta)\psi(\theta) \\
p(c) &= c + 8c^2\int \mathrm{d}\theta \sin(\theta)\int \mathrm{d}\theta' \sin(\theta')\psi(\theta)K(\theta,\theta')\psi(\theta') \\
\mu(c) &= f(c) + \frac{p(c)}{c},
\end{aligned}$$

with Z the normalisation constant. Note that introducing this external field gives rise to a temperature dependence, which was not present for the hard-rod interactions. All calculations for these systems have been performed using $N_\theta = N_\phi = 500$ and $\delta = 10^{-5}$. Figure 3.4 gives the dependence of a nematic $\psi(\theta)$ at $c = 4.5$ on the field strength. The field causes an asymmetry in the distribution by breaking the up-down symmetry. The rods possess a dipole moment giving them a preferential direction for the θ dependence of ψ, namely $\theta = 0$. The nematic director is pointed parallel to the field, as the dipole moments tend to align themselves along the field lines.

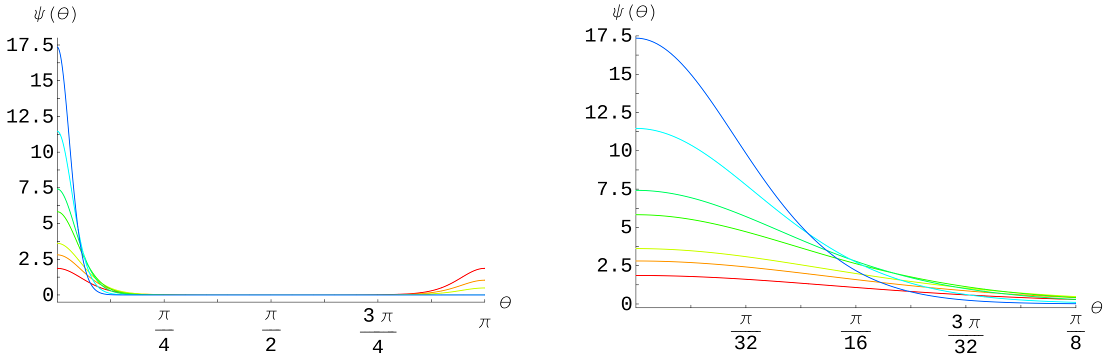

Figure 3.4: The orientation distribution $\psi(\theta)$ for the nematic phase with dimensionless concentration $c = 4.5$ at several dipolar field strengths (left). This field strength is represented by the dimensionless parameter βW, with the inverse temperature β and the interaction energy $W = mE$, where m is the (fixed) dipole moment and E the field strength. From red to blue: $\beta W = 0.0, 0.5, 1.0, 5.0, 10.0, 50.0$. Note the symmetry breaking, the red curve is completely symmetric, whilst the blue curve is completely asymmetric. Detail (right).

We can now determine the phase diagram for the field strength - concentration relation, figure 3.5 (left). There is a smooth transition from a state in which there is isotropic-nematic separation to a state in which the isotropic and nematic phases are indistinguishable. The critical point is located at $(c, \beta W) = (3.20, 0.742)$. This result indicates that smooth isotropic-nematic phase transition, via a field-concentration line clearing the coexistence curve. We refer to Appendix B for more results.

In figure 3.5 (right) the βW dependence of the isotropic and nematic S-value has been calculated for several concentrations. Note the almost linear behaviour of the nematic order parameter as a function of βW in the nematic phase. The isotropic phase responds more strongly to the introduction of an external field, exponentially instead of linearly. Nematic and isotropic branches exist simultaneously for c-values between $c = 3.5$ and $c = 4.0$, see figure 3.2 (right). However the isotropic branch for $c = 4.0$ is too small to be found by our approximation technique. Between these two c-values there is a linear drop-off in the βW for which the isotropic branch merges with the nematic one. The alignment of the rods with respect to the nematic director is a balance between the field, which tends to create order, and the entropy, which tends to maximise disorder. The isotropic phase interacts more strongly with the field because the entropy is not as as high as in the nematic phase. Yet it is the nematic phase which has the greatest c-variation in figure 3.5 (left). This seems a bit counter intuitive. We know the coexistence values of μ and p without an external field. By turning on the field, these values will increase in a similar way as S for a given concentration; exponentially and linearly. In practice it implies that both the isotropic and nematic phase need to have a lower concentration to obtain coexistence. Because the isotropic phase is more strongly influenced than the nematic phase, it does not need to decrease its c-value as much as the nematic to achieve coexistence. Only for quite high field strengths does the isotropic phase begin to experience entropic resistance to the field alignment, which in turn causes it to require higher concentrations for coexistence. This can be seen by the backward bending of the isotropic branch near the critical point.

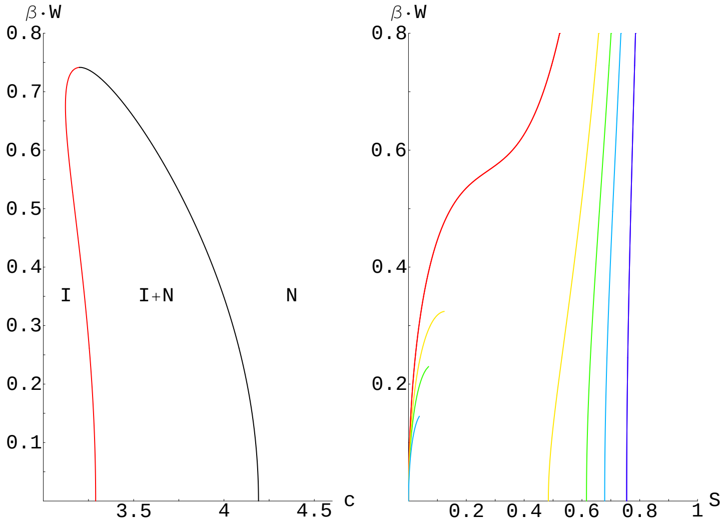

Figure 3.5: The field-concentration $(\beta W, c)$-phase diagram (left). The isotropic phase is represented in red and the nematic in black. There is a critical point at $(c, \beta W) = (3.20, 0.742)$. The nematic order parameter S as a function of βW for several c values (right). From red to blue $c = 3.25, 3.50, 3.625, 3.75, 4.00$. There is no colour distinction between the isotropic (leftmost) and nematic (rightmost) phases. The gaps in the yellow, green and light blue graph are caused by the almost horizontal tangent to the isotropic branch, causing the free energy minimisation routine to jump from the isotropic to a nematic phase in a single step. Note that the two phases occur simultaneously between $c = 3.5$ and $c = 4.0$, as we would expect form figure 3.2. For $c = 4.0$ only a nematic curve is visible, however there is an isotropic branch for $\beta W \approx 0$. It is too small to be found using the techniques employed in this thesis though. For the red curve a smooth isotropic-nematic phase transition can be observed.

The interplay between the field and the entropy is characterised by a steady decrease in S for the nematic coexistence c and a slightly more rapid increase in S for the isotropic coexistence c, see figure 5.6 (right) in Appendix B. Form this figure we obtain that $S_{\text{crit}} = 0.446$ at the critical point. The system is not completely aligned ($S = 1$) for this critical value though. This is because $\beta W = 0.742 < 1$, which implies that the field interaction energy is less than $k_B T$ and therefore it cannot be the dominant term in the nematic order parameter. In a rough estimate the field, causing ordering, and the ambient temperature, causing randomisation, contribute equally to S at the critical point, which yields $S_{\text{crit}} \approx 0.742/(0.742 + 1.000) = 0.43$. This indication of this S-value is quite reasonable considering that the actual value is given by $S_{\text{crit}} = 0.446$.

3.6 Limitations of this Model

We have examined the properties of monodisperse systems of dipolar hard colloidal rods. A graphical representation of the results has been given in the areas where the behaviour of the system is most interesting. Let us now investigate the limitations of this model. Obviously $L/D > 15/1$ is required for the second virial coefficient approximation to hold. However dipolar properties of the rods are of greater concern. The rods need to interact with a field in such a way that the dipole-dipole interactions contribute negligibly to the $B_2(\theta, \theta', \beta)$ and yet the field strength is not prohibitively high. If the dipole-dipole interactions are not negligible with respect to the hard-rod interactions, completely new phase types can occur. The tendency of the dipoles to form chainlike 'molecules' [13] results in one of these. Obviously the addition of dipolar moments will become increasingly noticeable for higher concentrations. Assume that the hard rods are mathematical dipoles with dipolar moment $\vec{m}$, then the dipole-dipole interaction potential is given by

$$I(\vec{r}, \vec{m}_1, \vec{m}_2) = \zeta \frac{\vec{m}_1 \cdot \vec{m}_2 - 3(\vec{m}_1 \cdot \hat{r})(\vec{m}_2 \cdot \hat{r})}{r^3} , \tag{3.17}$$

with ζ the interaction strength parameter. Consider the potential energy minima for dipole-dipole interactions, which give the configurations the system is most likely to assume if it is energy dominated. The first is a head to tail alignment of dipoles and the second is an antiparallel alignment, when the rods are side by side. Using equation (3.17), we find that these have interaction energy,

$$\begin{aligned} I_{\text{HT}} &= -\frac{2m^2\zeta}{r^3} && (3.18) \\ I_{\text{AP}} &= -\frac{m^2\zeta}{r^3} . && (3.19) \end{aligned}$$

For hard-rod systems there are three distances: $r = L$, for the head to tail configuration, $r = D$ for the antiparallel configuration and finally $r = \rho^{-1/3}$, which gives the average distance between the particles for a given number density $\rho = c/\mathcal{V}$. Substituting these distances in equations (3.18) and (3.19) results in four interaction energies

$$\begin{aligned} I_{\text{HT}} &= -\frac{2m^2\zeta}{L^3} && (3.20) \\ I_{\text{AP}} &= -\frac{m^2\zeta}{D^3} && (3.21) \\ I_{\text{HT, av}} &= -\frac{2m^2\zeta c}{\mathcal{V}} && (3.22) \\ I_{\text{AP, av}} &= -\frac{m^2\zeta c}{\mathcal{V}} . && (3.23) \end{aligned}$$

We use the condition $|I_{\text{dip-dip}}| \ll |I_{\text{field}}| = mE$ to indicate when the the dipole-dipole interactions become negligible compared to the field interaction. Using equations (3.20) through (3.23), ignoring equation

(3.22), one arrives at three estimates,

$$\begin{aligned}\frac{2\zeta m}{L^3} &\ll E\\ \frac{\zeta m}{D^3} &\ll E\\ \frac{\zeta m c}{\mathcal{V}} &\ll E.\end{aligned}$$

Let us examine the experimental feasibility of this type of system by estimating the E for which the dipole-dipole interactions are dominated by the field interaction; using known values for the dimensions and dipole moments of colloids. The typical dimensions of a colloidal rod, for instance those of the Tobacco Mosaic Virus, are $D \approx 20$ nm and $L \approx 300$ nm. For the value of the dimensionless concentration we use $c = \pi$, which is near the coexistence values and gives $4\zeta m/L^2 D \ll E$. The ζs for the magnetic and the electric dipole-dipole interactions are $\mu/4\pi$ (Tm/A) and $1/4\pi\epsilon$ (Vm/C) respectively. The magnetic dipole moments of certain types of bacteria are in the order of 10^{-15} Am^2, [14] and [15]. We take this value as an estimate for the magnetic dipole moment of a colloidal rod. The electric dipole moment of the colloids in Ref. [16] is $25 - 50$ Debye, which is equivalent to $\approx 10^{-28}$ Cm. A slightly larger value, namely 10^{-27} Cm, is used in the estimate given here. We can determine the field strength required by substituting the above mentioned quantities into our estimate. The three possibilities give an electric field of approximately $7 \cdot 10^2$, $1 \cdot 10^6$ and $2 \cdot 10^4$ V/m respectively, whereas the magnetic fields are given by $8 \cdot 10^{-3}$, 10 and 0.2 T respectively. Except for head to tail interactions, this is really considerable. Field strengths of 10 Tesla are not readily obtained in an average laboratory, and 10^6 V/m is quite close to the ionisation field strength of dry air, $3 \cdot 10^6$ V/m. This raises doubt on the feasibility of experimental verification. In addition the temperatures at which these experiments are performed needs to be taken into account. Consider an experiment at room temperature, 300 K, and colloidal rods with an electric dipole moment of 10^{-27} Cm. The range $0 \leq \beta m E \leq 1$ corresponds to an electric field of $0 \leq E \leq 4 \cdot 10^6$ V/m, which would be problematic if we require $E \gg 10^6$ V/m to overcome dipole-dipole dominance.

At first glance these estimates are troubling. However a more detailed analysis is required before we can definitively rule out the possibility of an experiment. Not all effects have been taken into account by this approximation, dipole screening by the solvent for instance. The estimate is quite rough and it is certainly possible that the dipole-dipole interactions do not have as strong an influence on the behaviour of the phases as determined here. Note that we have taken the inter-dipole distances to be close to the value for which the dipoles touch, if these distances are larger it would greatly reduce the field strengths required. The head to tail and the concentration distance estimates are more encouraging, but these might not be strong enough to be applicable to these systems.

Chapter 4

Onsager Theory for Bidisperse Suspensions of Rods

4.1 Theoretical Development

As before we may use the techniques employed by Onsager for bidisperse orientable systems, using a multi-species virial expansion. Take the external field to be directed along the $\hat{n}$-axis. Then the field interaction energies are $-W_1\langle\hat{\omega},\hat{n}\rangle$ and $-W_2\langle\hat{\omega},\hat{n}\rangle$ respectively, in inner product bracket notation. This results in the following expression in $\rho_1(\hat{\omega})$ and $\rho_2(\hat{\omega})$, were the ρ_i represent the density of component i,

$$\begin{aligned}
f(\rho_1,\rho_2) &= f_{\mathrm{id}}(\rho_1,\rho_2)+f_{\mathrm{sep}}(\rho_1,\rho_2)+f_{\mathrm{mix}}(\rho_1,\rho_2)+f_{\mathrm{ext}}(\rho_1,\rho_2)\\
f_{\mathrm{id}}(\rho_1,\rho_2) &= \int \mathrm{d}\hat{\omega}\rho_1(\hat{\omega})(\log(\rho_1(\hat{\omega})\mathcal{V}_1)-1)+\int \mathrm{d}\hat{\omega}\rho_2(\hat{\omega})(\log(\rho_2(\hat{\omega})\mathcal{V}_2)-1)\\
f_{\mathrm{sep}}(\rho_1,\rho_2) &= \int \mathrm{d}\hat{\omega}\int \mathrm{d}\hat{\omega}'\rho_1(\hat{\omega})B_2^{(11)}(\hat{\omega},\hat{\omega}',\beta)\rho_1(\hat{\omega}')+\int \mathrm{d}\hat{\omega}\int \mathrm{d}\hat{\omega}'\rho_2(\hat{\omega})B_2^{(22)}(\hat{\omega},\hat{\omega}',\beta)\rho_2(\hat{\omega}')\\
f_{\mathrm{mix}}(\rho_1,\rho_2) &= 2\int \mathrm{d}\hat{\omega}\int \mathrm{d}\hat{\omega}'\rho_1(\hat{\omega})B_2^{(12)}(\hat{\omega},\hat{\omega}',\beta)\rho_2(\hat{\omega}')\\
f_{\mathrm{ext}}(\rho_1,\rho_2) &= -\beta W_1\int \mathrm{d}\hat{\omega}\rho_1(\hat{\omega})\langle\hat{\omega},\hat{n}\rangle-\beta W_2\int \mathrm{d}\hat{\omega}\rho_2(\hat{\omega})\langle\hat{\omega},\hat{n}\rangle\\
B_2^{(xy)}(\hat{\omega},\hat{\omega}',\beta) &= -\frac{1}{2}\int \mathrm{d}\vec{r}(\exp(-\beta\phi(\vec{r}_{(xy)},\hat{\omega},\hat{\omega}')-1).
\end{aligned}$$

Now introduce the following notations make the formulae more appealing, with x the composition parameter: $\rho_1=(1-x)\rho$, $\rho_2=x\rho$, $L_i=\lambda_i L$, $D_i=\delta_i D$, $\mathcal{V}_i=\pi L_i^2 D_i/4$, $\mathcal{V}=\pi L^2 D/4$, $\rho_i\psi_i(\theta)=\rho_i(\hat{\omega})$ and $c=\mathcal{V}\rho$. For a system where particle species 1 has a field interaction strength $W_1=m_1E$ and species

2 interaction parameter $W_2 = m_2 E$, we write $f(c,x) = \beta F/N$ as

$$\begin{aligned}
f(c,x) &= f_{\mathrm{id}}(c,x) + f_{\mathrm{sep}}(c,x) + f_{\mathrm{mix}}(c,x) + f_{\mathrm{ext}}(c,x) \\
f_{\mathrm{id}}(c,x) &= \log(c) - 1 + (1-x)\log(1-x) + x\log(x) + \log(\lambda_1^2\delta_1) + x\log\left(\frac{\lambda_2^2\delta_2}{\lambda_1^2\delta_1}\right) \\
&\quad +2\pi(1-x)\int \mathrm{d}\theta \sin(\theta)\psi_1(\theta)\log(\psi_1(\theta)) + 2\pi x\int \mathrm{d}\theta \sin(\theta)\psi_2(\theta)\log(\psi_2(\theta)) \\
f_{\mathrm{sep}}(c,x) &= 8c\lambda_1^2\delta_1(1-x)\int \mathrm{d}\theta \sin(\theta)\int \mathrm{d}\theta' \sin(\theta')\psi_1(\theta)K(\theta,\theta')\psi_1(\theta') \\
&\quad +8c\lambda_2^2\delta_2 x\int \mathrm{d}\theta \sin(\theta)\int \mathrm{d}\theta' \sin(\theta')\psi_2(\theta)K(\theta,\theta')\psi_2(\theta') \\
f_{\mathrm{mix}}(c,x) &= 8c\lambda_1\lambda_2(\delta_1+\delta_2)x(1-x)\int \mathrm{d}\theta \sin(\theta)\int \mathrm{d}\theta' \sin(\theta')\psi_1(\theta)K(\theta,\theta')\psi_2(\theta') \\
f_{\mathrm{ext}}(c,x) &= -2\pi(1-x)\beta W_1\int \mathrm{d}\theta \sin(\theta)\psi_1(\theta)\cos(\theta) - 2\pi x\beta W_2\int \mathrm{d}\theta \sin(\theta)\psi_2(\theta)\cos(\theta).
\end{aligned}$$

This yields the following conditions for the equilibrium distributions

$$\begin{aligned}
\psi_1(\theta) &= \frac{1}{Z_1}\exp\left(-\frac{8c}{\pi}\lambda_1^2\delta_1(1-x)\int \mathrm{d}\theta' \sin(\theta')\psi_1(\theta')K(\theta,\theta')\right) \\
&\quad \times\exp\left(-\frac{4c}{\pi}\lambda_1\lambda_2(\delta_1+\delta_2)x\int \mathrm{d}\theta' \sin(\theta')\psi_2(\theta')K(\theta,\theta')\right) \\
&\quad \times\exp\left(\beta W_1\cos(\theta)\right) \\
\psi_2(\theta) &= \frac{1}{Z_2}\exp\left(-\frac{8c}{\pi}\lambda_2^2\delta_2 x\int \mathrm{d}\theta' \sin(\theta')\psi_2(\theta')K(\theta,\theta')\right) \\
&\quad \times\exp\left(-\frac{4c}{\pi}\lambda_1\lambda_2(\delta_1+\delta_2)(1-x)\int \mathrm{d}\theta' \sin(\theta')\psi_1(\theta')K(\theta,\theta')\right) \\
&\quad \times\exp\left(\beta W_2\cos(\theta)\right) \\
p(c,x) &= c^2\left(\frac{\partial f}{\partial c}\right)(c,x) \\
\mu_1(c,x) &= f(c,x) + \frac{p(c,x)}{c} - x\left(\frac{\partial f}{\partial c}\right)(c,x) \\
\mu_2(c,x) &= f(c,x) + \frac{p(c,x)}{c} + (1-x)\left(\frac{\partial f}{\partial c}\right)(c,x).
\end{aligned}$$

Here the Z_i are normalisation constants. The definition of S is unchanged, but there are two S values now, one for each component of the system. When $\psi_1(\theta) = \psi_2(\theta) = 1/4\pi$, we can re-write the equations above as

$$\begin{aligned}
f(c,x) &= \log(c/4\pi) - 1 + (1-x)\log(1-x) + x\log(x) + \log(\lambda_1^2\delta_1) + x\log\left(\frac{\lambda_2^2\delta_2}{\lambda_1^2\delta_1}\right) \\
&\quad +c\lambda_1^2\delta_1(1-x)^2 + c\lambda_2^2\delta_2 x^2 + c\lambda_1\lambda_2(\delta_1+\delta_2)x(1-x) \qquad (4.1) \\
p(c,x) &= c + c^2\lambda_1^2\delta_1(1-x)^2 + c^2\lambda_2^2\delta_2 x^2 + c^2\lambda_1\lambda_2(\delta_1+\delta_2)x(1-x). \qquad (4.2)
\end{aligned}$$

These equations are only relevant for $W_1 = W_2 = 0$. The functions μ_1 and μ_2 follow directly from equations (4.1) and (4.2) and are omitted here. For the nematic fieldless case there also exist expansions at high densities see Ref. [17]. Having obtained expressions for the physical parameters, we proceed to discuss the numerical techniques used to approximate them in the next section.

4.2 Numerical Results without an External Field Interaction

The iteration scheme can be readily generalised to include two functions, $\psi_1(\theta)$ and $\psi_2(\theta)$, for which self-consistency is required. Modification of the Newton-Raphson procedure is more involved however. Recall that for the monodisperse case a system of two unknown variables, on which two conditions are imposed, needed to be solved. In a bidisperse system the unknowns are c_1^*, c_2^*, x_1^* and x_2^*, with the conditions $p(c_1^*, x_1^*) = p(c_2^*, x_2^*)$, $\mu_1(c_1^*, x_1^*) = \mu_1(c_2^*, x_2^*)$ and $\mu_2(c_1^*, x_1^*) = \mu_2(c_2^*, x_2^*)$. This is a system of 3 equations with 4 variables, which implies some freedom of choice. To solve this problem, introduce the dimensionless pressure p, and rewrite the system as $p(c_1^*, x_1^*) = p$, $p(c_2^*, x_2^*) = p$, $\mu_1(c_1^*, x_1^*) = \mu_1(c_2^*, x_2^*)$ and $\mu_2(c_1^*, x_1^*) = \mu_2(c_2^*, x_2^*)$. A 4D NR-procedure can be applied to this system of four equations in four variables. As we will see in the next sections, varying p and finding coexistence conditions will lead to some interesting results.

Let us first examine the bidisperse system without involving field interactions. All the results here were generated using the following parameters, $N_\theta = N_\phi = 150$ and $\delta = 10^{-6}$. The number of considered pressures p per graph is 100 for the fieldless case, but can increase or decrease for the field strength slices. At the endpoints of certain field slices $N_\theta = N_\phi = 300$ and $\delta = 10^{-7}$ was used. We have chosen to consider the following system: $\lambda_1 = \lambda_2 = \delta_1 = 1$ and $\delta_2 = 3$, i.e. the rods have equal length and a diameter ratio of 1/3. This choice may seem arbitrary, as any conceivable configuration is possible. However, this thin-thick diameter ratio has already been investigated in Ref. [17] and [18], which is used to verify our results before introducing a field dependence. This $D_1/D_2 = 1/3$ case has an interesting phase diagram and nematic-nematic coexistence phenomena do not noticeably affect the nematic phase. These phenomena do affect the higher ratio systems considerably [17]. In addition, it is quite difficult to create pure systems, there is always some dispersion in man-made colloids. A factor of three gives us a difference between the two types well outside this natural dispersion. For example, a system with $D_1/D_2 = 1/1.1$ does not possess sufficient difference between the two components, to be readily created in a laboratory. Furthermore NR experiences great difficulty in finding phase coexistence for these ratios.

We consider only the coexistence phenomena for bidisperse systems in this thesis. The non-coexistence forms for the pressure, chemical potentials etc. are interesting, but there are too many parameters to give an accurate description of the entire system within the limitations of 2D representations. Using only the coexistence values in our representation, the parameter space is conveniently reduced. Figure 4.1 shows the phase diagrams for $D_1/D_2 = 1/3$ without an external field. There are two phases coexisting with each other, each with its own composition and concentration. For a given p we can take a horizontal line and determine the intersection with both the red and the black curve in the graphs, giving us the (x, c, p) for both phases.

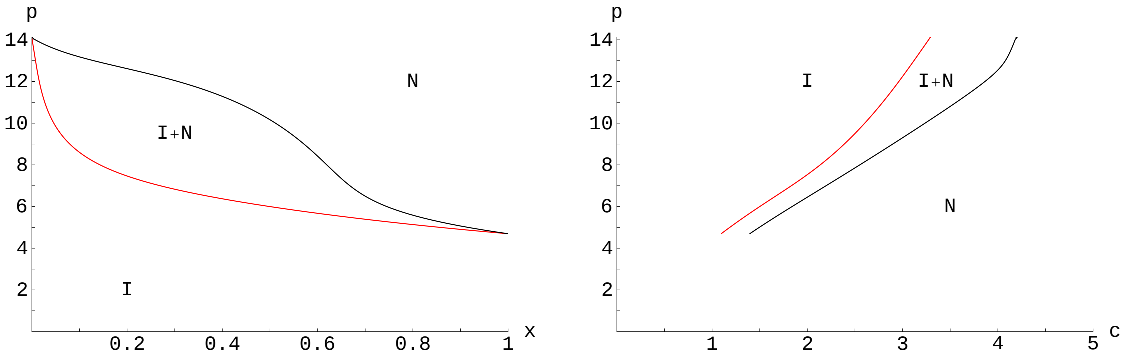

Figure 4.1: The pressure-composition (p, x)-phase diagram (left) and the pressure-concentration (p, c)-phase diagram (right) for a bidisperse system of colloidal rods with a diameter ratio $D_1/D_2 = 1/3$. The red curve represents the isotropic phase, the black curve the nematic phase.

The endpoints for (x, p) are $(0, 14.12)$ and $(1, 4.506)$. For $(c_1, c_2; p)$ the endpoints are $(3.290, 4.191; 14.12)$

and $(1.097, 1.397; 4.506)$. The values given here have numerical precision of ± 0.004. Note that the latter values are exactly $(1/3)$ of the initial values, which follows from our chosen diameter ratio. In addition there is exact correspondence with the monodisperse coexistence parameters. We estimate that for all points there is a fractional uncertainty of less than 0.035%. This value is obtained by comparing the pressure p for which NR is to find coexistence with the p values NR returns. Using figure 4.2 one can conclude that the (red) phase is isotropic and the (black) nematic. There is a strong fractionation at coexistence between the isotropic phase and the nematic phase. The nematic phase is relatively rich in thick rods and the isotropic relatively rich in thin ones. The reason behind this fractionation is the relatively large excluded volume in interactions of thick rods, which makes them more susceptible to orientational ordering [19]. It can be shown that this fractionation is strongly dependent on the diameter ratio [17]. See Appendix C for the coexistence data of the f, μ_1 and μ_2; the red and black curve overlap for μ_1 and μ_2, within the numerical precision, which is one of the coexistence requirements.

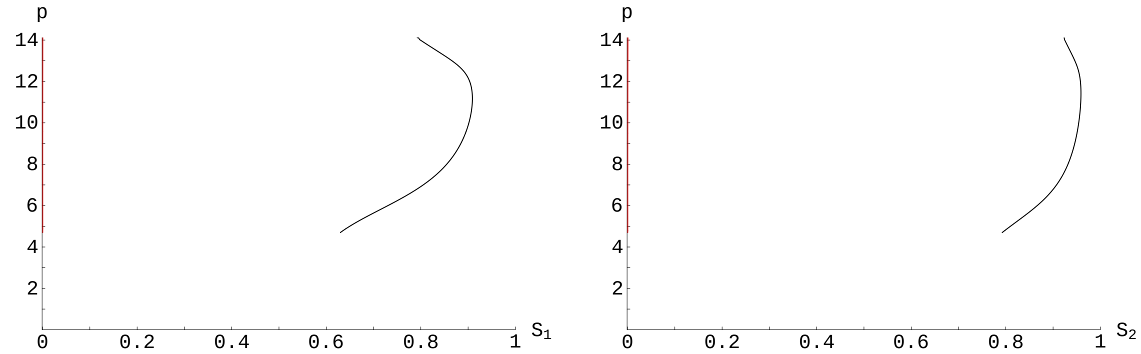

Figure 4.2: The nematic order parameters for a bidisperse system of colloidal rods with a diameter ratio $D_1/D_2 = 1/3$. S_1 for the orientation distribution $\psi_1(\theta)$ of the thin particles (left) and S_2 for the orientation distribution $\psi_2(\theta)$ of the thick rods (right) as function of the dimensionless pressure p. The red curve represents the isotropic phase, the black curve the nematic phase.

4.3 Numerical Results with an External Field Interaction

Before considering the field dependence of bidisperse systems of colloidal rods let us return to the monodisperse case and regard the pressure dependence of the coexistence curve in figure 3.5 (left). As this curve will form the boundary of the (p, c)-phase diagram for the top endpoints of figure 4.1 (right); for the bottom, c and p values have to be divided by three. For the (p, x)-phase diagram, figure 5.5 (right) in Appendix B gives the boundary at $x = 0$ and $x = 1$, where for $x = 1$ again the p value has to be divided by three. In a three dimensional representation the monodisperse coexistence curve is given by figure 4.3.

Now we may describe the results for a bidisperse system, with $W_1/W_2 = 1/1$. The 1/1 ratio has been chosen for technical reasons, i.e. the smallest gaps and no NR convergence issues in other parts of the graph. We refer to Appendix D for some additional results with $W_1/W_2 = 1/2$ and $W_1/W_2 = 1/3$. Because the pictures are in fact three dimensional, slices parallel to the (p, x)-plane and (p, c)-plane have been used. This results in a (p, x)- and a (p, c)-phase diagram respectively, with a 2D level set representation structure. We have also taken $(\beta W_1, x)$- and $(\beta W_1, x)$-slices, resulting in the respective $(\beta W_1, x)$- and $(\beta W_1, c)$-phase diagrams.

The choice of the slices may seem a bit arbitrary for the (p, x)- and (p, c)-representation. The steep nature of the (p, c)-phase diagram, figure 3.5 (left) and the $(\beta W_1, c)$-diagram figure 4.5 (right), as well as that of the $(\beta W_1, x)$-phase, figure 4.4 (right), forces us to use non-equidistant level sets. The number of slices in the $(\beta W_1, x)$- and $(\beta W_1, c)$-representation has been kept to a minimum to prevent the phase-diagrams from becoming too cluttered. We have also chosen not to include the boundaries of the

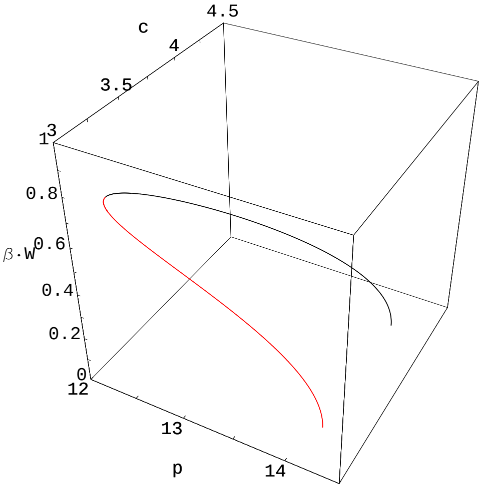

Figure 4.3: The field-concentration $(\beta W, c)$-phase diagram for a monodisperse system of colloidal rods. The dimensionless pressure p at which coexistence is achieved, for a given c and βW, has been included to obtain a 3D shape. Again the red curve represents the isotropic phase and the black curve the nematic phase.

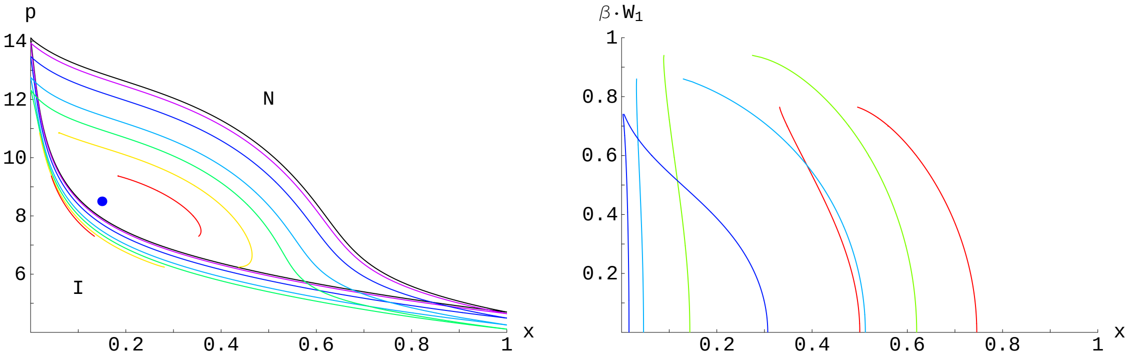

Figure 4.4: The pressure-composition (p, x)-phase diagram (left) and the field-composition $(\beta W_1, x)$-phase diagram (right) for a bidisperse system of colloidal rods with diameter ratio $D_1/D_2 = 1/3$ and a dipole moment ratio given by $W_1/W_2 = 1/1$. From black to red the dimensionless field strength parameter $\beta W_1 = 0.0$, 0.2, 0.4, 0.6, 0.7, 0.8 and 0.9, in the (p, x)-phase diagram. The isotropic phase is the bottom left and the nematic phase the top right curve for each colour. There appears to be a critical value of $\beta W_1^* \leq 1$ at $(x, c, p) \approx (0.15 \pm 0.05, 2.5 \pm 0.1, 8.5 \pm 0.5)$, where the uncertainty is given in standard deviation notation. This point has been indicated using a blue dot. Note that this maximum is about 35% higher than the critical value for monodisperse systems, namely $\beta W = 0.742$; a phenomenon which is caused by fractionation. For the $(\beta W_1, x)$-phase diagram, red $p = 6$, green $p = 8$, light blue $p = 10$ and dark blue $p = 12$. The isotropic phase is the left and the nematic phase the right line for each colour.

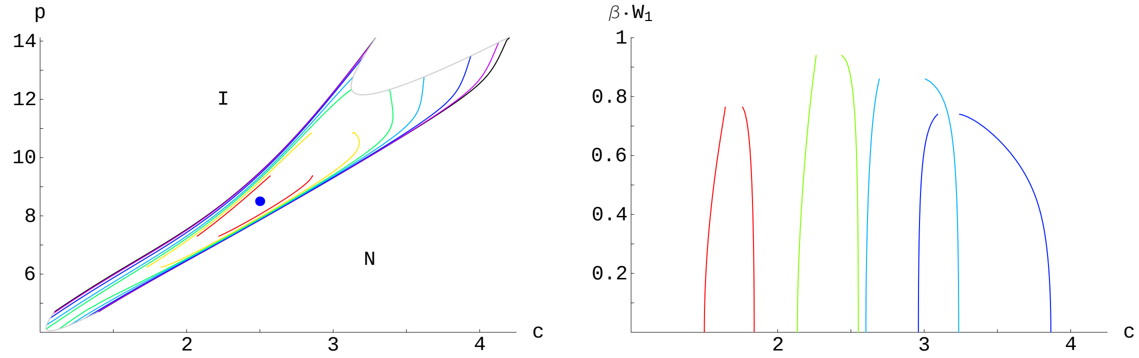

Figure 4.5: The pressure-concentration (p, c)-phase diagram (left) and the field-concentration $(\beta W_1, c)$-phase diagram (right) for a bidisperse system of colloidal rods with diameter ratio $D_1/D_2 = 1/3$ and a dipole moment ratio given by $W_1/W_2 = 1/1$. From black to red the dimensionless field strength parameter $\beta W_1 = 0.0$, 0.2, 0.4, 0.6, 0.7, 0.8 and 0.9, in the (p, c)-phase diagram. The grey curve is the boundary imposed by the monodisperse limit to the system. The isotropic phase is the top left and the nematic phase the bottom right curve for each colour. A blue dot indicates the estimated position of the critical point. For the $(\beta W_1, c)$-phase diagram, red $p = 6$, green $p = 8$, light blue $p = 10$ and dark blue $p = 12$. The isotropic phase is the left and the nematic phase the right line for each colour.

monodisperse limit for the same reason. Closing the graphs is exceedingly difficult, if not impossible using the techniques employed here, which explains the presence of the gaps in the phase slices. The Jacobi matrix probably has a large inverse with respect to its Euclidean matrix norm at the top of the separation zone. This makes the NR-procedure susceptible to computer precision inaccuracies and causes its step-size to increase near the coexistence points, rather than decrease. As stated above these unclosed slices are a compilation of several segments, where increasing precision was used for the segments close to the endpoints.

The coexistence curves seem to deform smoothly. The separation zone in figure 4.4 appears to be bounded by a value of $\beta W_1^* \leq 1$, with its maximum at $(x, c, p) \approx (0.15 \pm 0.05, 2.5 \pm 0.1, 8.5 \pm 0.5)$ where the uncertainty is given in standard deviation notation. Note that this maximum is about 35% higher than the value $\beta W = 0.742$. The increase of the critical field strength from its value in the monodisperse system correlates with the width of the fractional gap between the curves. The presence of the small fraction of thicker rods allows for an increase in the entropy effect. The critical value is a balance between entropy, tending to make the system disordered, and field alignment. Because the presence of the thick rods increases the entropy, a higher field strength is required to achieve the critical value, where the isotropic phase is sufficiently aligned to be indistinguishable from the nematic phase for all c, x and p. The isotropic (p, c)-curve is affected far less by the field than the nematic one, by the same reasons as given for the monodisperse system in section 3.5. We may conclude that there is a critical line, the crest of this 3D shape, below which there is nematic-isotropic phase separation for the corresponding p-value. This means there can be a smooth isotropic-nematic phase transition, via a field-concentration line which clears the separation zone at a given pressure.

In figure 4.4 and 4.5, no slices have been included from $\beta W_1 \in]0.7, 0.8[$, where the monodisperse system has a critical point, namely at $\beta W_1 = \beta W_2 = 0.742$. Upon further examination of this range we find the behaviour given by figure 4.6. Note that the curves have a tendency to close even below the critical value of 0.742. The lines have not been continued beyond their terminal point, because the NR-routine does not converge there or it produces dubious results. At $\beta W_1 = 0.73$ there is an almost vertical tangent to the nematic curve, a sign of the coexistence curve splitting into two parts. At $\beta W_1 = 0.72$ there is still a looping back tendency, the little hook on the end consists of 7 NR-points with a fractional uncertainty of less then 0.01%. In addition, figures 5.11 (right) and 5.12 (right) in Appendix D show that the red curve at $p = 6$ terminates around $\beta W_2 = 3\beta W_1 = 0.63 \sim 0.65$, well below the monodisperse critical

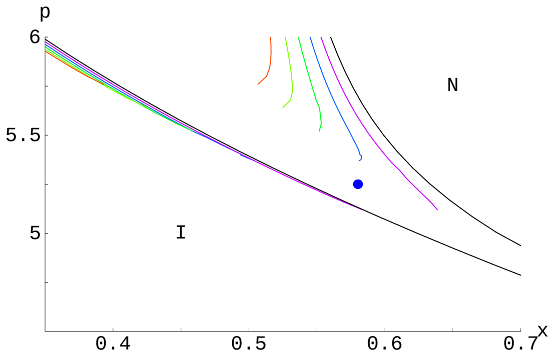

Figure 4.6: An enlargement of the pressure-composition (p, x)-phase shown in figure 4.4 (left). This section gives the critical zone in which backward bending nematic phase lines indicate the possibility of a saddle point. If this is indeed the case, the saddle point can be found at $(x, c, p) \approx (0.58 \pm 0.07, 1.4 \pm 0.1, 5.25 \pm 0.25)$, indicated using a blue dot. From black to red the dimensionless field strength parameter $\beta W_1 = 0.70$, 0.71, 0.72, 0.73, 0.74 and 0.75.

value of $\beta W_2 = 3\beta W_1 = 0.742$ for $x = 1$. This leads us to believe that there might be a saddle point on the boundary of the separation zone. Note that this behaviour does not appear to occur in figures 5.9 (right) and 5.10 (right) for $W_1/W_2 = 1/2$, which could be attributed to the location of the slices. An explanation for the presence of such a saddle point would require further theoretical analysis of this system, but it is probably caused by some complicated interplay of entropy, fractionisation and field strength.

Unfortunately a saddle point has one of the worst NR convergence properties of all curvatures, and attempts to find it have so far been unsuccessful. If such a point does exist then it will have coordinates $(x, c, p) \approx (0.58 \pm 0.07, 1.4 \pm 0.1, 5.25 \pm 0.25)$. However it could also be the case, although we deem this to be less likely, that the phase curve does not split into two disjoined parts for level sets between $\beta W_1 \approx 0.72$ and $\beta W_1 \approx 0.74$. Then the thin point in which the phase diagram terminates for x near 1, becomes thinner and thinner, eventually vanishing smoothly around $\beta W_1 \approx 0.742$. This does require us to find some other explanation for the vertical tangent lines and the low critical value at $W_1/W_2 = 1/3$ for $p = 6$. Calculation of these phenomena are well outside the domain of numerical uncertainty.

The results described above lead us to believe that there are interesting qualities to the mathematics of Onsager's theory in the second virial approximation for bidisperse systems. We must however not loose perspective, this approximation only works for high L/D ratio's. By introducing a second species of particle with a diameter three times as large as the first, the length of the first particle should be least 45 times its diameter. Also note that the dipole-dipole interactions become more important as one of the species interacts stronger with the field than the other, in case of $W_1/W_2 = 1/3$, the $1 - 2$ coupling increases by a factor 3 and that of the $2 - 2$ by a factor of 9. Therefore the approximation, for $W_1/W_2 \neq 1/1$, is going to loose accuracy and relevance quickly. Especially considering the remarks made earlier concerning the feasibility of these negligible dipole-dipole interaction systems in section 3.6.

Chapter 5

Summary and Discussion

We have given a theoretical development of Onsager theory in this thesis. Starting form a non-ideal gas virial expansion, a semi-grand canonical formalism for solutions and suspensions was derived. Onsager's second virial coefficient approximation for systems of particles with a directional dependence followed form these results. This theory was applied to a monodisperse system of colloidal rods, yielding a non-linear integral equation for the directional distribution function. An analysis of the mathematics of this equation was presented and numerical approximation schemes were used to find the solution. The isotropic and nematic phase for monodisperse systems of colloidal rods have been rigorously investigated. An exact correspondence between mathematical and numerical results was shown for the isotropic phase and for the position of the isotropic-nematic branching point as calculated by Kayser and Raveché. Phase coexistence properties were determined using a Newton-Raphson technique. The influence of an external dipolar field on this coexistence has also been examined and a critical point was found at $\beta W = 0.742$. Finally the methods applied to monodisperse systems were extended to allow the analysis of bidisperse rod suspensions.

For these bidisperse suspensions we have chosen to restrict attention to thick and thin rods, i.e. rods of equal length ($L_1/L_2 = 1/1$) and diameter ratio $D_1/D_2 = 1/3$. With the introduction of an external field the dipole moment ratios $W_1/W_2 = 1/1$, $W_1/W_2 = 1/2$ and $W_1/W_2 = 1/3$ were considered. The behaviour of these systems mirrors that of monodisperse ones, in the sense that there is phase separation in both cases. This separation can be nullified in a continuous manner using an external field, which makes the phases indistinguishable at sufficiently high βW values. For a dipole moment ratio of $W_1/W_2 = 1/1$, the critical value above which there is no separation for all x, c and p is about 35% higher than the critical value for monodisperse systems. This increase can be attributed to fractionation. We speculate that there is one remarkable feature of the critical line/crest in $W_1/W_2 = 1/1$ systems. Isotropic-nematic merging appears to occur at lower βW than expected from the results obtained for monodisperse systems, hinting at the possibility of a saddle point on the boundary of the separation zone. If this is indeed the case, the appearance of such a saddle point would require theoretical foundation and mathematical derivation.

There is a lot of room for further research in this area. We have examined only a fraction of the choices available. One can take any value for λ_1, λ_2, δ_1, δ_2, W_1, W_2 and take any form for the Φ_{ext}. One possibility, a second Legendre polynomial type field interaction, is being considered by M.G.A. van Dorp using techniques similar to those employed here. For the specific case of a dipole field interaction, investigating the existence or absence of a saddle point is a good starting point. One might also study the behaviour of the phase coexistence relations when the ratio W_1/W_2 is changed smoothly from 1/1 to 1/3 for instance. The three phase diagrams produced in this thesis for $W_1/W_2 = 1/1$, 1/2 and 1/3 are not sufficient to make meaningful statements about the nature of this phase diagram - dipole ratio relation. Producing three dimensional images of the results could prove informative, but with the number of slices used here, the results we obtained were unsatisfactory. Of course other phases could be considered, such as smectic, columnar and crystalline. This addition would lead to phase diagrams of even greater complexity. One should start this investigation for the $W_1 = W_2 = 0$ case; to our knowledge this type of research has not been performed yet. For $W_1 = W_2 = 0$, the behaviour of isotropic-nematic and nematic-nematic coexistence as a function of the diameter ratio is known. The influence of an external field on these coexistence relations can be regarded as well.

Finally there is room for experimental verification of the results, although this would most definitely be a qualitative analysis considering the nature of this model. The 35% increase in critical value for the bidisperse maximum is an effect which could probably be measured. There are significant obstacles to be overcome though. A $D_1/D_2 = 1/3$ system has been created under laboratory conditions, but ensuring that both rod types have a dipole moment such that it satisfies the conditions from section 3.6 would pose a challenge.

Acknowledgements

It is a pleasure to thank M.G.A. van Dorp, a Bachelor student at the Utrecht University, who contributed to the realisation of this thesis. I also wish to convey my gratitude to Dr. R.H.H.G. van Roij, who supervised this project and proofread this manuscript, for his patience and support.

Bibliography

[1] C. Kittel and H. Kroemer. *Thermal Physics.* W.H. Freeman and Company, 2nd edition, 1980.

[2] M. Dijkstra and R. Van Roij. *Thermische Fysica 2 (Blok 2)*, pages 27–28,45–46. Lecturenotes Utrecht University, 2005.

[3] J.E. Mayer and M.G. Mayer. *Statistical Mechanics*, pages 263–267,277–294,454–467. John Wiley And Sons Inc., 8th edition, 1959.

[4] O.K. Rice. *Statistical Mechanics, Thermodynamics and Kinetics*, pages 240–269. W.H. Freeman and Company, 1st edition, 1967.

[5] R. Aldrovandi and I. Monte Lima. A matricial approach to cluster expansions. *J. Phys. A: Math. Gen.*, 13:3685–3696, 1980.

[6] R. Van Roij. *Thermische Fysica 2*, pages 37–43,59–63,69–76. Lecturenotes Utrecht University, 2003.

[7] L. Onsager. The effects of shape on the interaction of colloial particles. *Ann. N. Y. Acad. Sci.*, 51: 627–659, 1949.

[8] D.H. Griffel. *Applied Functional Analysis.* Dover Publications, 1st edition, 2002.

[9] R.F. Kayser and H.J. Raveché. Bifurcation in Onsager's model of the isotropic-nematic transition. *Physical Review A*, 17:2067–2072, 1978.

[10] R. Van Roij. The isotropic and nematic liquid crystal phase of colloidal rods. *Eur. J. Phys.*, 26: s57–s67, 2005.

[11] G.J. Vroege and H.N.W. Lekkerkerker. Phase transitions in lyotropic colloidal and polymer liquid crystals. *Rep. Prog. Phys.*, 55:1241–1309, 1992.

[12] W.H. Press, B.P. Flannery, S.A. Teukolsky, and W.T. Vetterling. *Numerical Recipes in C : The Art of Scientific Computing*, pages 379–383. Cambridge University Press, 2nd edition, 1992.

[13] P.I.C. Teixeira. Phase diagrams of aligned dipolar hard rods. *Physical Review E*, 57:1752–1760, 1998.

[14] R.E. Dunin-Borkowski, M.R. McCartney, R.B. Frankel, D.A. Bazylinski, M. Pósfai, and P.R. Buseck. Magnetic Microstructure of Magnetotactic Bacteria by Electron Holography. *Science*, 282:1868–1870, 1998.

[15] R.B. Frankel, R.P. Blakemore, and R.S. Wolfe. Magnetite in Freshwater Magnetotactic Bacteria. *Science*, 203:1355–1356, 1979.

[16] S.A. Blanton, R.L. Leheny, M.A. Hines, and P. Guyot-Sionnest. Dielectric Dispersion Measurements of CdSe Nanocrystal Colloids: Observation of a Permanent Dipole Moment. *Physical Review Letters*, 79:865–868, 1997.

[17] R. Van Roij, B. Mulder, and M. Dijkstra. Phase behavior of binary mixtures of thick and thin hard rods. *Physica A*, 261:374–390, 1998.

[18] K. Shundyak and R. Van Roij. Free planar isotropic-nematic interfaces in binary hard-rod fluids. *Physical Review E*, 68:4789–4800, 2003.

[19] H.N.W. Lekkerkerker, Ph. Coulon, R. Van Der Haegen, and R. Deblieck. On the isotropic nematic liquid crystal phase separation in a solution of rodlike particles of different lengths. *J. Chem. Phys.*, 80:3427–3433, 1984.

[20] H.N.V. Temperley. On the mutual cancellation of cluster integrals in Mayers's fugacity series. *Proc. Phys. Soc.*, 83:3–15, 1964.

[21] H.H. Chen. Weak lattice constants and the virial expansion for a classical gas. *J. Phys. A: Math. Gen.*, 17:197–209, 1984.

[22] I. Fatkullin and V. Slastikov. A note on the Onsager model of nematic phase transitions. *Comm. Math. Sci.*, 3:21–26, 2005.

[23] K.R. Prudy, V. Szabolcs, A. Galindo, G. Jackson, and S. Fraden. Nematic Phase Transitions in Mixtures of Thin and Thick Colloidal Rods. *Physical Review Letters*, 94:7801–7805, 2005.

[24] H.H. Wensink and G.J. Vroege. Nematic order of model goethite nanorods in a magnetic field. *Physical Review E*, 72:1708–1717, 2005.

Appendix A

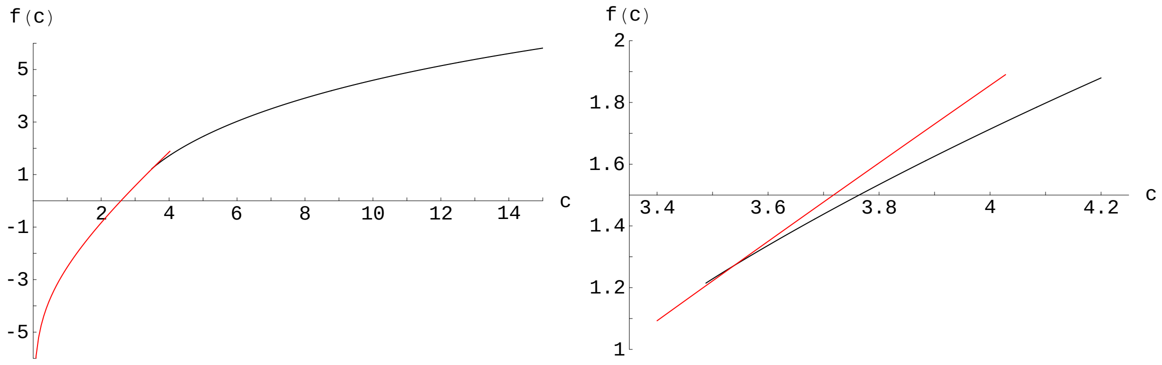

Figure 5.1: The dimensionless free energy $f(c)$ as a function of the dimensionless concentration c for a monodisperse system of colloidal rods (left). The red curve represents the isotropic phase, the black curve the nematic phase. Detail (right).

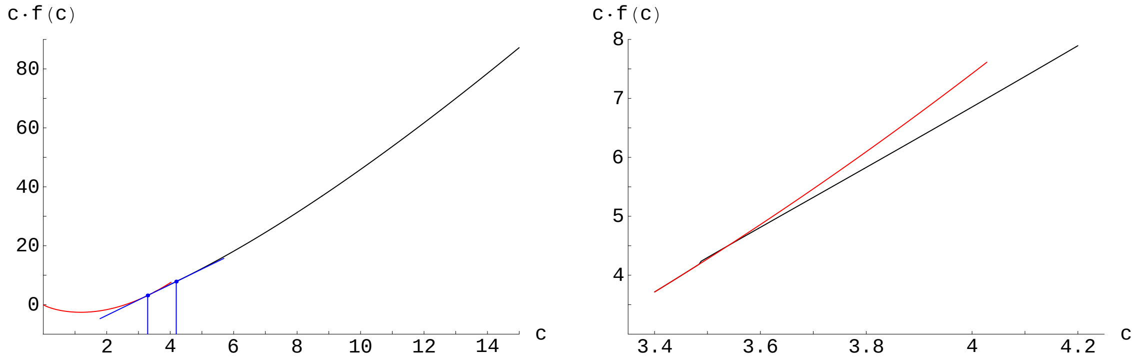

Figure 5.2: The dimensionless scaled free energy $cf(c)$ as a function of the dimensionless concentration c for a monodisperse system of colloidal rods (left). A Maxwell common tangent construction has been applied to this graph, given by the blue line. The vertical blue lines are used to indicate the position of the coexistence points. Detail (right). Note the insignificant variation in the tangent on this domain.

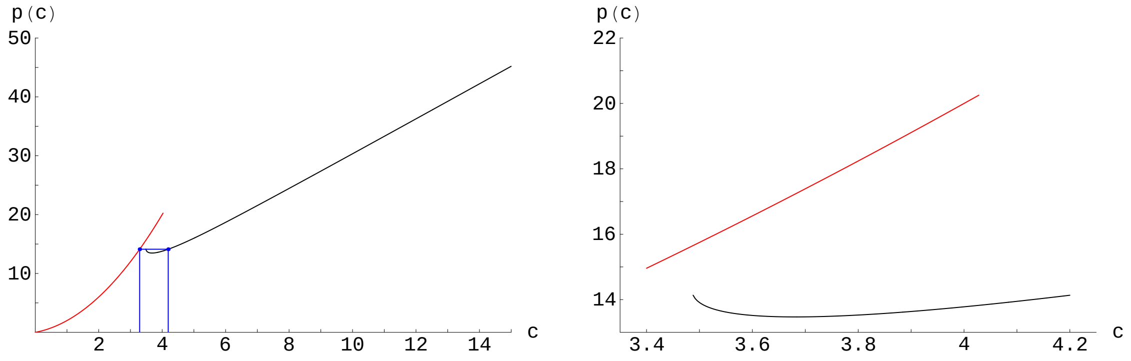

Figure 5.3: The dimensionless pressure $p(c)$ as a function of the dimensionless concentration c for a monodisperse system of colloidal rods (left). The coexistence points have been indicated in blue, the horizontal line indicates that the pressures in both phases are equal at coexistence. Detail (right).

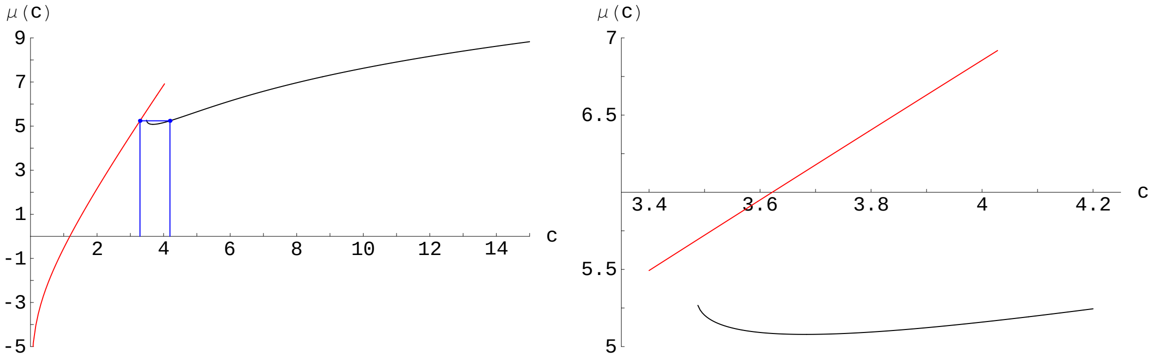

Figure 5.4: The dimensionless chemical potential $\mu(c)$ as a function of the dimensionless concentration c for a monodisperse system of colloidal rods (left). The coexistence points have been indicated in blue. Detail (right).

Appendix B

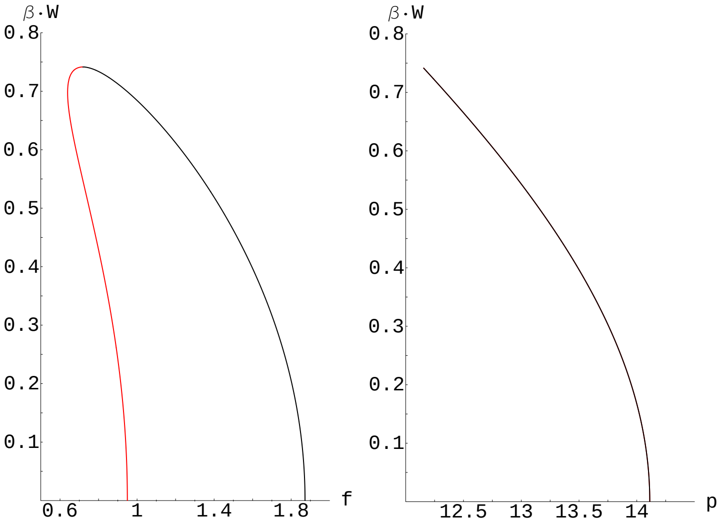

Figure 5.5: The coexistence dimensionless free energy f (left) and the coexistence dimensionless pressure p (right) for a monodisperse system of colloidal rods as a function of the dimensionless field strength parameter βW. The red curve represents the isotropic phase, the black curve the nematic phase. The red and black curve overlap for the pressure diagram, a condition for phase coexistence.

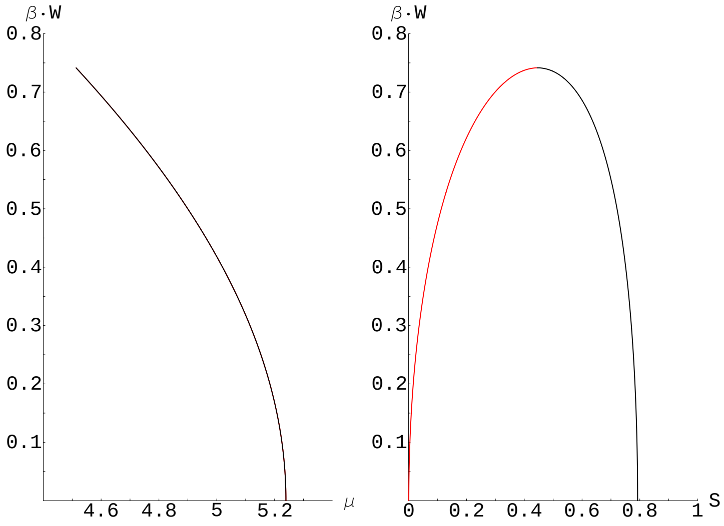

Figure 5.6: The the coexistence dimensionless chemical potential μ (left) and the coexistence nematic order parameter S (right) for a monodisperse system of colloidal rods as a function of the dimensionless field strength parameter βW. The red and black curve overlap for the chemical potential, as is required for coexistence.

Appendix C

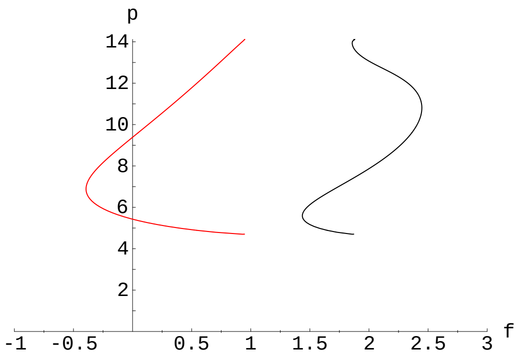

Figure 5.7: The dimensionless free energy f as function of the dimensionless pressure p for a bidisperse system of colloidal rods with a diameter ratio $D_1/D_2 = 1/3$. The red curve represents the isotropic phase, the black curve the nematic phase.

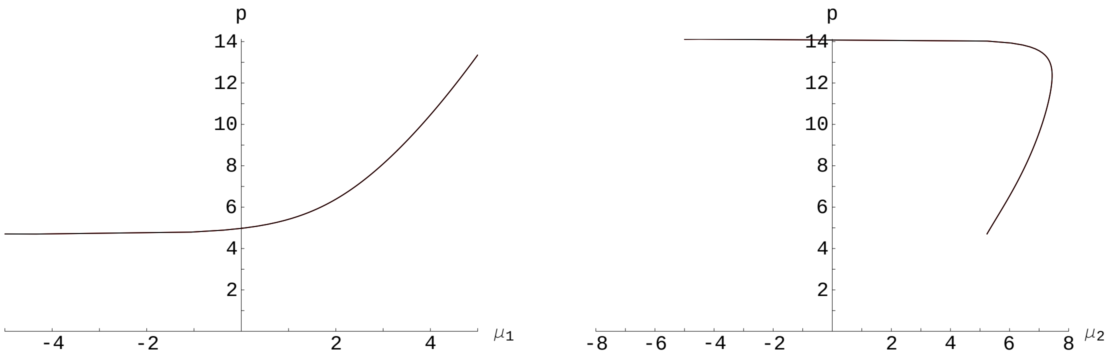

Figure 5.8: The dimensionless chemical potentials for a bidisperse system of colloidal rods with a diameter ratio $D_1/D_2 = 1/3$. The μ_1 (left) for the thin rods and the μ_2 (right) for the thick rods as function of the dimensionless pressure p. Note that the black curve overlaps the red curve completely, as is required for isotropic-nematic coexistence.

Appendix D

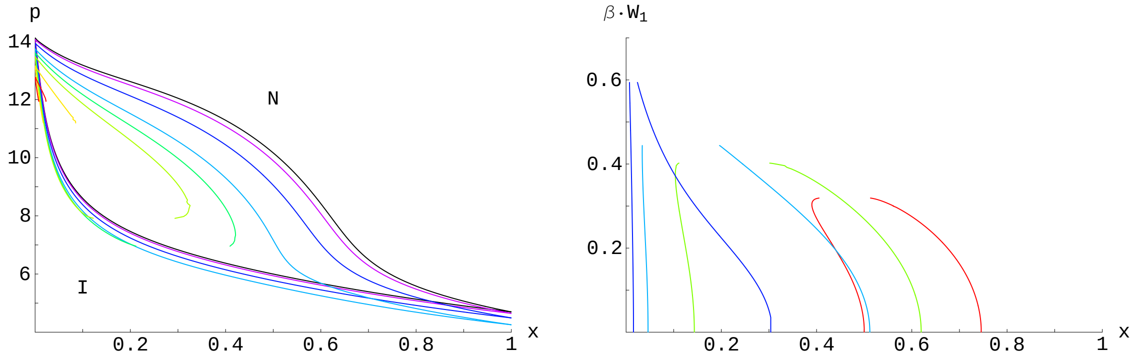

Figure 5.9: The pressure-composition (p, x)-phase diagram (left) and the field-composition $(\beta W_1, x)$-phase diagram (right) for a bidisperse system of colloidal rods with diameter ratio $D_1/D_2 = 1/3$ and a dipole moment ratio given by $W_1/W_2 = 1/2$. From black to red the dimensionless field strength parameter $\beta W_2 = 2\beta W_1 = 0.0$, 0.2, 0.4, 0.6, 0.7, 0.8, 1.0 and 1.2, in the (p, x)-phase diagram. The isotropic phase is the bottom left and the nematic phase the top right curve for each colour. For the $(\beta W_1, x)$-phase diagram, red $p = 6$, green $p = 8$, light blue $p = 10$ and dark blue $p = 12$. The isotropic phase is the left and the nematic phase the right line for each colour.

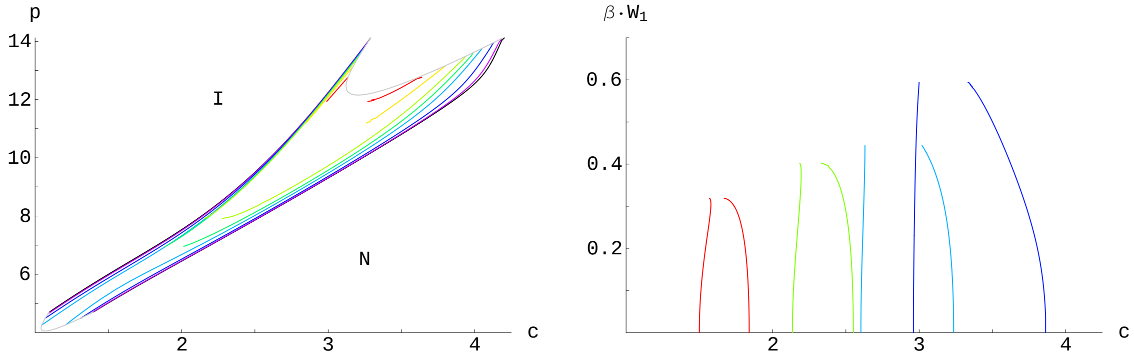

Figure 5.10: The pressure-concentration (p, c)-phase diagram (left) and the field-concentration $(\beta W_1, c)$-phase diagram (right) for a bidisperse system of colloidal rods with diameter ratio $D_1/D_2 = 1/3$ and a dipole moment ratio given by $W_1/W_2 = 1/2$. From black to red the dimensionless field strength parameter $\beta W_2 = 2\beta W_1 = 0.0$, 0.2, 0.4, 0.6, 0.7, 0.8, 1.0 and 1.2, in the (p, c)-phase diagram. The grey curve is the boundary imposed by the monodisperse limit to the system. The isotropic phase is the top left and the nematic phase the bottom right curve for each colour. For the $(\beta W_1, c)$-phase diagram, red $p = 6$, green $p = 8$, light blue $p = 10$ and dark blue $p = 12$. The isotropic phase is the left and the nematic phase the right line for each colour.

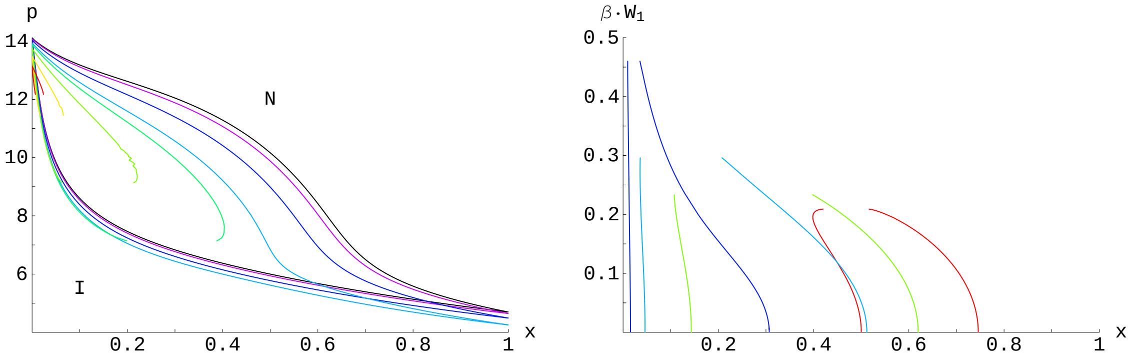

Figure 5.11: The pressure-composition (p, x)-phase diagram (left) and the field-composition $(\beta W_1, x)$-phase diagram (right) for a bidisperse system of colloidal rods with diameter ratio $D_1/D_2 = 1/3$ and a dipole moment ratio given by $W_1/W_2 = 1/3$. From black to red the dimensionless field strength parameter $\beta W_2 = 3\beta W_1 = 0.0$, 0.2, 0.4, 0.6, 0.7, 0.9, 1.2 and 1.5, in the (p, x)-phase diagram. For the $(\beta W_1, x)$-phase diagram, red $p = 6$, green $p = 8$, light blue $p = 10$ and dark blue $p = 12$. Note the unexpectedly low value for which the red curve terminates. Around $3\beta W_1 = 0.63 \sim 0.65$, well below the monodisperse critical value of $\beta W_2 = 3\beta W_1 = 0.742$.

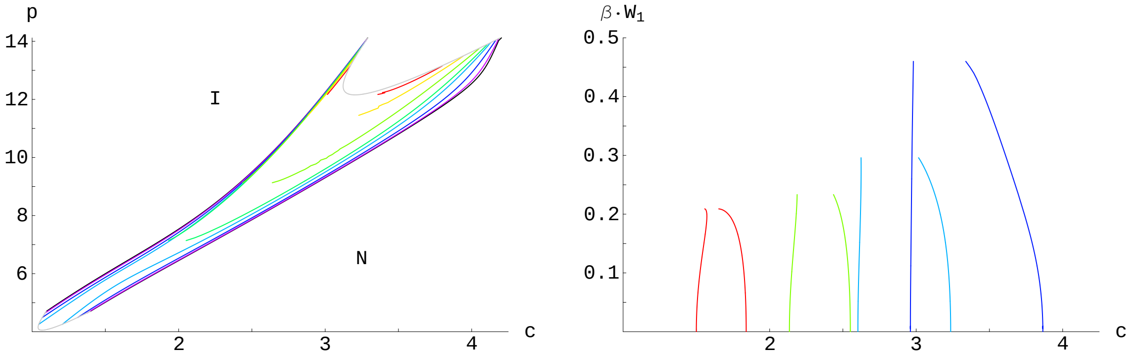

Figure 5.12: The pressure-concentration (p, c)-phase diagram (left) and the field-concentration $(\beta W_1, c)$-phase diagram (right) for a bidisperse system of colloidal rods with diameter ratio $D_1/D_2 = 1/3$ and a dipole moment ratio given by $W_1/W_2 = 1/3$. From black to red the dimensionless field strength parameter $\beta W_2 = 3\beta W_1 = 0.0$, 0.2, 0.4, 0.6, 0.7, 0.9, 1.2 and 1.5, in the (p, c)-phase diagram. For the $(\beta W_1, c)$-phase diagram, red $p = 6$, green $p = 8$, light blue $p = 10$ and dark blue $p = 12$. Again we have this unexpectedly low red curve.